

Formation and Evolution of Dwarf Elliptical Galaxies - II. Spatially resolved star-formation histories

Mina Koleva^{1,2*}, Sven De Rijcke³, Philippe Prugniel¹, Werner W. Zeilinger⁴,
Dolf Michielsen³,

¹ *Université Lyon 1, Villeurbanne, F-69622, France; CRAL, Observatoire de Lyon, St. Genis Laval, F-69561, France ; CNRS, UMR 5574*

² *Department of Astronomy, St. Kliment Ohridski University of Sofia, 5 James Bourchier Blvd., BG-1164 Sofia, Bulgaria*

³ *Sterrenkundig Observatorium, Ghent University, Krijgslaan 281, S9, B-9000 Ghent, Belgium*

⁴ *Institut für Astronomie, Universität Wien, Türkenschanzstrasse 17, A-1180 Wien, Austria*

Accepted 2009 03 23. Received 2009 03 16; in original form 2008 11 19

ABSTRACT

We present optical VLT spectroscopy of 16 dwarf elliptical galaxies (or dEs) comparable in mass to NGC 205, and belonging to the Fornax cluster and to nearby groups of galaxies. Using full-spectrum fitting, we derive radial profiles of the SSP-equivalent ages and metallicities. We make a detailed analysis with ULYSS and STECKMAP of the star-formation history in the core of the galaxies and in an aperture of one effective radius. We resolved the history into 1 to 4 epochs. The statistical significance of these reconstructions were carefully tested; the two programs give remarkably consistent results.

The old stellar population of the dEs, which dominates their mass, is likely coeval with that of massive ellipticals or bulges, but the star formation efficiency is lower. Important intermediate age (1-5 Gyr) populations, and frequently tails of star formation until recent times are detected. These histories are reminiscent of their lower mass dSph counterparts of the Local Group.

Most galaxies (10/16) show significant metallicity gradients, with metallicity declining by 0.5 dex over one half-light radius on average. These gradients are already present in the old population. The flattened (or discy), rotating objects (6/16) have flat metallicity profiles. This may be consistent with a distinct origin for these galaxies or it may be due to their geometry. The central SSP-equivalent age varies between 1 and 6 Gyr, with the age slowly increasing with radius in the vast majority of objects. The group and cluster galaxies have similar radial gradients and star-formation histories.

The strong and old metallicity gradients place important constraints on the possible formation scenarios of dEs. Numerical simulations of the formation of spherical low-mass galaxies reproduce these gradients, but they require a longer time for them to build up. A gentle depletion of the gas, by ram-pressure stripping or starvation, could drive the gas-rich, star-forming progenitors to the present dEs.

Key words: galaxies: dwarf - galaxies : formation and evolution - galaxies : stellar populations

1 INTRODUCTION

Diffuse ellipticals, or dwarf elliptical galaxies (dEs), are small, low-luminosity galaxies ($M_B \gtrsim -18$ mag) (Ferguson & Binggeli 1994). They are among the most numerous galaxy species in the universe. Being found typically not more than a few hundred kiloparsecs away from a

massive galaxy or in groups and clusters of galaxies, they show a strong predilection for high-density environments. Their diffuse, approximately exponentially declining surface-brightness profiles set them apart from the compact ellipticals (cEs) which, while occupying the same luminosity range as the dEs, have much higher central surface brightnesses and a de Vaucouleurs-like surface-brightness profile (Kormendy 1985; Nieto & Prugniel 1987; Kormendy et al. 2008; but see Graham & Guzmán 2003).

* E-mail: mina.koleva@obs.univ-lyon1.fr

The star formation and metal enrichment history are likely not regular, as star formation may be both triggered and quenched by environmental effects (Mayer et al. 2001; Haines et al. 2007; van den Bosch et al. 2008). Moreover, dEs may not be a homogeneous population. There is tempting evidence that at least part of the dE population evolved from more late-type, gas-rich progenitors. This includes the occurrence of dEs with a rotation velocity that is compatible with them being isotropic oblate rotators (De Rijcke et al. 2001; Prugniel & Simien 2003; van Zee et al. 2004) and dEs with kinematically decoupled cores and/or embedded stellar discs and bars (Jerjen et al. 2000; Barazza et al. 2002; Graham et al. 2003; De Rijcke et al. 2003a, 2004; Chilingarian et al. 2007; Lisker et al. 2007). High-speed gravitational interactions with giant galaxies within the dense group or cluster environment may be sufficient to induce the morphological transformation of a discy dwarf irregular galaxy into a much rounder dwarf spheroidal (dSph) or dwarf elliptical galaxy (Moore et al. 1998; Mayer et al. 2001; Mastropietro et al. 2005). Some dEs still contain an interstellar medium (Young & Lo 1997; De Rijcke et al. 2003b; Michielsen et al. 2004; Buyle et al. 2005; Bouchard et al. 2007) and host ongoing star formation (De Rijcke et al. 2003b; Lisker et al. 2006; Michielsen et al. 2007).

Detailed information about the star formation histories of a representative sample of dEs is instrumental in elucidating their origin and evolution. In the first paper of this series (De Rijcke et al. 2005, Paper I), we compared simulations of the evolution of dEs with observed scaling relations, such as the Faber-Jackson relation and the Fundamental Plane. We found good agreement with models based on the premise that dEs are primordial objects whose dark-matter halo merging time-scale is shorter than the star-formation time-scale and in which supernova explosions play an important role in regulating star formation and moving gas around. Part of the data used in Paper I was collected in the course of an ESO Large Programme on the internal kinematics of dEs (program ID 165.N-0115). In the present paper, we use deep long-slit spectra to probe the composition of the stellar populations and the star-formation histories of the same sample of dEs as in Paper I. This sample contains dEs with kinematically decoupled cores and embedded discs and spiral structures whose stellar populations can be compared with those of *prima facie* primordial dEs.

In section 2, we describe the sample of 16 objects, the observations, and the data reduction. In section 3, we present the radial profiles of SSP-equivalent ages and metallicities. Section 4 contains a detailed analysis of the stellar populations in the nuclei and main bodies of the targeted galaxies and a reconstruction of the star-formation histories in these two zones. We finalize with a discussion of the results in section 5 and summarize our conclusions in section 6.

2 OBSERVATIONS AND DATA REDUCTION

2.1 The sample

The sample consists of 16 dEs, 9 in the Fornax cluster, 4 in the NGC 5044 group, two in the NGC 5898 group and one in the Antlia (NGC 3258) group. Structural properties of the

Table 2. Characteristics of the galaxy groups from which the sample was composed. Columns 2 & 3: Mean radial velocity relative to the CMB and velocity dispersion listed in HyperLeda, <http://leda.univ-lyon1.fr>, (Paturel et al. 2003) calculated as in Prugniel et al. (1999). Columns 4 & 5: Distance modulus, assuming $H_0 = 72 \text{ km s}^{-1}/\text{Mpc}$, and radial scale for 1 arcsec at the corresponding distance. Column 6: Central bright-galaxy density, measured by $\log(\Sigma_5)$ (see eq. (1)).

group/cluster	$\langle cz \rangle$ km s^{-1}	σ km s^{-1}	mod	r pc	$\log(\Sigma_5)$
NGC5898 group	2390	145	32.60	160	-0.7
Fornax cluster	1540	285	31.65	104	0.5
NGC5044 group	2700	210	32.87	182	0.7
NGC3258 group	2860	280	33.00	193	1.4

objects are listed in Table 1. They are essentially comparable to NGC 205, the most luminous being about 6 times brighter than this prototype. The galaxies are ordered according to the importance of their old population, as determined later in this study (Sect. 4.1), starting with those most dominated by the old population (i. e. the shortest formation time-scale).

We have collected photometric data of dSphs/dEs from the galaxy groups and clusters represented in our sample. Analogous to Goto et al. (2003), we quantify the galaxy densities of these environments as the projected density of galaxies brighter than $M_B = -19$ mag within the radius d_5 that contains five such galaxies, or:

$$\Sigma_5 = \frac{5}{\pi d_5^2} \text{ galaxies Mpc}^{-2}. \quad (1)$$

The $\log(\Sigma_5)$ -values and other characteristics of the different environments are listed in Table 2.

The NGC5898 group constitutes the sparsest environment covered by the dataset (it consists of two bright ellipticals, NGC5903 and NGC5898, and a few tens of much fainter galaxies; Gourgoulhon et al. 1992 list only three group members brighter than $M_B \approx -18$ mag). The Fornax cluster and the NGC5044 group have comparable bright galaxy densities and can be considered to be similar environments, significantly denser than the NGC5898 group. The Antlia cluster has a densely populated core, reflected by its high $\log(\Sigma_5)$ value.

The spectroscopic observations were carried out during two ESO-VLT service mode runs. The group dEs were observed in April – May 2005 using FORS2 and the Fornax dEs were observed in December 2005 – January 2006 using FORS1. The setup of the observations is summarized in Table 3. Exposure times are listed in Table 4. During the observations, the seeing conditions varied from FWHM = 0.5 to 0.8 arcsec. We also observed three velocity and metallicity standards for each run; two of which belong to the Lick/IDS and the MILES stellar libraries (Sánchez-Blázquez et al. 2006). The data reduction, described in detail below, was performed using the ESO-MIDAS data reduction software package.

Table 1. Structural properties of the observed dEs (taken from De Rijcke et al. (2005)).

name	α (J2000) (hms)	δ (J2000) (dms)	m_B (mag)	ϵ^a	σ (km s $^{-1}$)	R_e (arcsec)	$\mu_{e,B}$ (mag arcsec $^{-2}$)	Sérsic n	type	comment
FCC136	03 34 29.5	-35 32 47	14.81	0.21	64.3 \pm 3.8	14.2	22.57	1.71	dE2	
FCC266	03 41 41.4	-35 10 12	15.90	0.11	42.4 \pm 3.4	7.1	22.15	1.08	dE0,N	
FCC150	03 35 24.1	-36 21 50	15.70	0.19	63.8 \pm 3.9	5.7	21.48	1.65	dE4,N	
FCC245	03 40 33.9	-35 01 23	16.00	0.11	39.5 \pm 4.2	11.4	23.28	1.35	dE0,N	
NGC5898_DW1	15 18 13.0	-24 11 47	15.66	0.34	43.5 \pm 3.0	8.7	22.35	1.53	dE3	
FS029	13 13 56.2	-16 16 24	15.70	0.54	59.6 \pm 3.6	8.9	22.44	1.79	dE5	
FS373	10 37 22.9	-35 21 37	15.60	0.23	73.1 \pm 3.1	7.9	22.03	2.71	dE3	KDC
FS076	13 15 05.9	-16 20 51	16.10	0.07	56.8 \pm 3.8	4.4	21.41	2.02	dE1	KDC
FCC288	03 43 22.6	-33 56 25	15.10	0.72	48.5 \pm 3.3	9.5	21.99	1.11	dS0	spiral
FS131	13 16 49.0	-16 19 42	15.30	0.54	87.0 \pm 3.2	8.1	21.83	2.35	dE5,N	peanut
FS075 ^b	13 15 04.1	-16 23 40	16.87	0.10	49 \pm 6	6.8	23.03	1.74	dE1,N	
FCC207	03 38 19.3	-35 07 45	16.19	0.15	60.9 \pm 6.6	8.4	22.81	1.32	dE2,N	H α emission
NGC5898_DW2	15 18 44.7	-24 10 51	16.10	0.57	44.2 \pm 3.4	5.9	21.95	1.26	dS0,N	emission
FCC204	03 38 13.6	-33 07 38	14.76	0.61	67.2 \pm 4.4	11.5	22.06	1.29	dS0	spiral
FCC043	03 26 02.2	-32 53 40	13.91	0.26	56.4 \pm 3.7	16.9	22.05	2.17	dE3	
FCC046	03 26 25.0	-37 07 41	15.99	0.36	61.4 \pm 5.0	6.7	22.12	1.24	dE4,N	H α , H α emission

^a $\epsilon = 1 - b/a$, with b/a the minor to major axis ratio of the isophotes

^b not observed in ESO Large Programme 165.N-0115; the velocity dispersion is a preliminary value obtained with the current data, its relatively large error bar is due to the uncertainty on the instrumental line-spread function.

Table 3. Setup of observations

	FORS 1	FORS 2
VLT unit	Kueyen (UT2)	Antu (UT1)
CCD	Tektronix	2 MIT mosaic
# of pixels	2k \times 2k	2k \times 4k (2 \times 2 binned)
pixel size (μm^2)	24 \times 24	30 \times 30
image scale (arcsec pix $^{-1}$)	0.20	0.25
readout noise (e $^{-}$ pix $^{-1}$)	5.6	3.15
gain (ADU (e $^{-}$) $^{-1}$)	0.71	1.43
FORS grism	GRIS_600B+22	GRIS_1200g+96
slit width (arcsec)	0.5	1.0
spectral range (\AA)	3300 – 6200	4355 – 5640
FWHM $\Delta\lambda$ (\AA)	2.6	3.0
σ_{instr} (km s $^{-1}$ @ 5200 \AA)	64	74

2.2 FORS2 observations

The calibration data include bias frames, dome flat-field frames, and wavelength calibration frames which were taken during the day before and after the observations. During twilight of each night, spectrophotometric standard stars were observed, using a 5 arcsec slit. For three nights we did not have calibration data, in which case we took the frames from the following night. The bias frames for each night (typically 10) were averaged and then median filtered over a box of 5 \times 5 pixels. The dome flat frames (typically 5) were bias subtracted, normalized and averaged. The resulting frame was median filtered over 40 pixels in the wavelength direction in order to yield the variation of the intensity of the dome lamp with wavelength. The small-scale flat-field was computed by dividing the averaged by the median filtered frame. We also took twilight flats which were bias subtracted, flat-fielded, average combined and averaged along the wavelength direction to measure the variation of the illumination along the slit (spatial direction). Because of the very high S/N there

was no need to approximate this function with a polynomial. The small-scale flat-field was multiplied by the normalized slit transfer function to yield a master flat frame.

The wavelength calibration was done on He-Hg-Cd arc frames observed with the same setup. Fitting a two-dimensional dispersion relation using two-dimensional 4th-order polynomials yielded an overall accuracy of 0.06 \AA r.m.s. or ~ 3.6 km s $^{-1}$ at 5000 \AA . The wavelength calibrated frames were all rebinned to a common 1.5 \AA pix $^{-1}$ wavelength scale.

The FORS2 data show quite strong distortions of more than 3 pixels over the whole wavelength range. In order to correct it, we determined the variation of the spatial centre of the bluest standard star, and fitted a 3rd order polynomial along the wavelength range. We chose the bluest standard star because the quantum efficiency of the CCD in the blue part is not very high and the centre of the objects are very difficult to determine except in this star. Applying this correction to the other spectra, we noted a significant residual linear distortion. This was fitted in the red part of the spectrum where the centre is well defined and then added to the original 3rd order polynomial to make one resampling correcting the distortion to better than 0.02 arcsec r.m.s.

Each science frame was bias-subtracted and flat-fielded. Then we removed the cospics by first applying the MIDAS FILT/COS command and subsequently inspecting all the frames by eye to remove low-intensity cospics missed by the routine. Then we corrected for the slit distortion as described above. After that the frames were wavelength calibrated and rectified. Sky subtraction was performed by fitting the regions of the spectrum empty of target light contributions with a linear relation. Each frame was corrected for extinction using the extinction coefficients provided by ESO and the mean of the airmass at the start and end of each exposure. The spectra were flux-calibrated using the spectrophotometric standard stars and spectral images of the same object were co-added.

Table 4. Observation log

galaxy name	FORS (1/2)	t_{obs} (s)	P.A. slit ($^{\circ}$)
FCC 043	1	4×960	80
FCC 046	1	3×1900	80
FCC 136	1	4×960	172
FCC 150	1	3×1900	10
FCC 204	1	3×1900	22
FCC 207 ^a	1	4×2280	114
FCC 245 ^b	1	14×1300	10
FCC 266	1	4×2280	10
FCC 288 ^c	1	4×2280	4
FS 29	2	6×1300	98
FS 75	2	4×1300	0
FS 76	2	4×1300	36
FS 131	2	4×1300	131
FS 373	2	4×1300	97
NGC 5898 DW1	2	10×1300	174
NGC 5898 DW2	2	14×1300	12

^a 1 exposure excluded (clouds)

^b 1 exposure excluded (seeing > 2 arcsec FWHM)

^c 1 exposure excluded (clouds)

The error spectra were calculated by transporting the photon and read-out noises through all the steps of the data reduction.

2.3 FORS1 observations

The reduction of the FORS1 data is identical to that of the FORS2 observations, except for the following steps: For the wavelength calibration we used 12 lines. We fitted a two-dimensional dispersion relation using polynomials of order 3 and 5 in wavelength and spatial scale respectively, to an accuracy of 0.03 Å rms or $\sim 2 \text{ km s}^{-1}$ at 5000 Å. The frames were rebinned to 0.6 Å pixel^{-1} . The FORS1 CCD shows negligible distortion ($< 0.05 \text{ arcsec}$), which was not corrected.

2.4 Analysis of the individual exposures

Before co-adding the different exposures we analysed their central 1 arcsec extraction in order to check their internal consistency. In order to minimize the change of the line-spread function (LSF, the analogous of the PSF in the wavelength direction), we fitted the line-of-sight velocity distribution (LOSVD), the age and the metallicity in a short wavelength range (4310 – 4400 Å in rest-frame). We identified some exposures producing slightly discrepant results, mostly for the LOSVD but also for the population parameters. Checking the ambient conditions from the ESO meteo monitoring, we found that these exposures were taken in worse seeing conditions than requested.

Only for 3 galaxies did the derived kinematics and stellar population parameters differ significantly from frame to frame. In one case - FS29 - the seeing changed from 0.6 arcsec to almost 1.8 arcsec FWHM over the series of exposures. We excluded therefore the last exposure of the series,

in order to preserve the high resolution in the co-added spectrum. For the other 10 galaxies the seeing variations were, although measurable, not significant.

We also notice that many exposures (especially for FORS2 observations) were taken with a seeing smaller than the slit width. As shown by the different instrumental broadening measured on the twilight spectra (uniform lightening of the slit) and on the calibration stars, this has a significant effect on the measurement of the LOSVD. As we will see later, our analysis methods fits in the same time the LOSVD and the parameters of the population. In the present case, the velocity and velocity dispersion are likely biased and we will not discuss them. However, in order to suppress the metallicity – velocity dispersion degeneracy (Koleva et al. 2008b), the LOSVD will be free parameters of our analysis.

2.5 Extraction of 1D spectra

For each object, we extract two 1D spectra integrated within simulated elliptical apertures with major axes equal to 0.5 arcsec and 1 effective radius, R_e .

Assuming the slit width to be negligible, a spectrum at a distance r_i along the slit is supposed to be representative of the semi-ellipse with major axis r_i and with ellipticity ϵ (for which we take the galaxy’s mean ellipticity). If each pixel measures Δr arcseconds on the sky, a spectrum at a distance r from the galaxy centre is then weighted with a factor $2\pi r(1 - \epsilon)\Delta r$ in the extracted spectrum, \mathcal{F} . A radial bin at radius r_i starts at $r_i - 0.5\Delta r$ and ends at $r_i + 0.5\Delta r$. We then find for the extracted spectrum that

$$\mathcal{F}_\lambda = 2\pi\Delta r \sum_i F_{i,\lambda} r_i, \quad (2)$$

with $F_{i,\lambda}$ the observed spectrum at a distance r_i from the centre, and in the noise on the extracted spectrum, \mathcal{N} ,

$$\mathcal{N}_\lambda = \sqrt{\sum_i (2\pi\Delta r)^2 r_i^2 N_{i,\lambda}^2}, \quad (3)$$

with $N_{i,\lambda}$ the noise on the observed spectrum at a distance r_i from the centre.

The central extraction is approximately the seeing disc and corresponds to a diameter between 104 and 182 pc for the various objects of the sample (see Table 2). This extraction is likely essentially sensitive to the population in the core, while the external extraction, within $1 R_e$ and excluding the inner 1 arcsec region, can be considered as representative of the galaxy’s main body.

3 RADIAL PROFILES OF THE POPULATION PARAMETERS

In this section, after describing the method used to determine them, we present the radial profiles of the age and metallicity of the galaxies. Then we measure these characteristics in the central regions, after correction of the light contamination projected along the line of sight.

3.1 Analysis method

The principle of our analysis is to compare an observed spectrum with a model of a population broadened to ac-

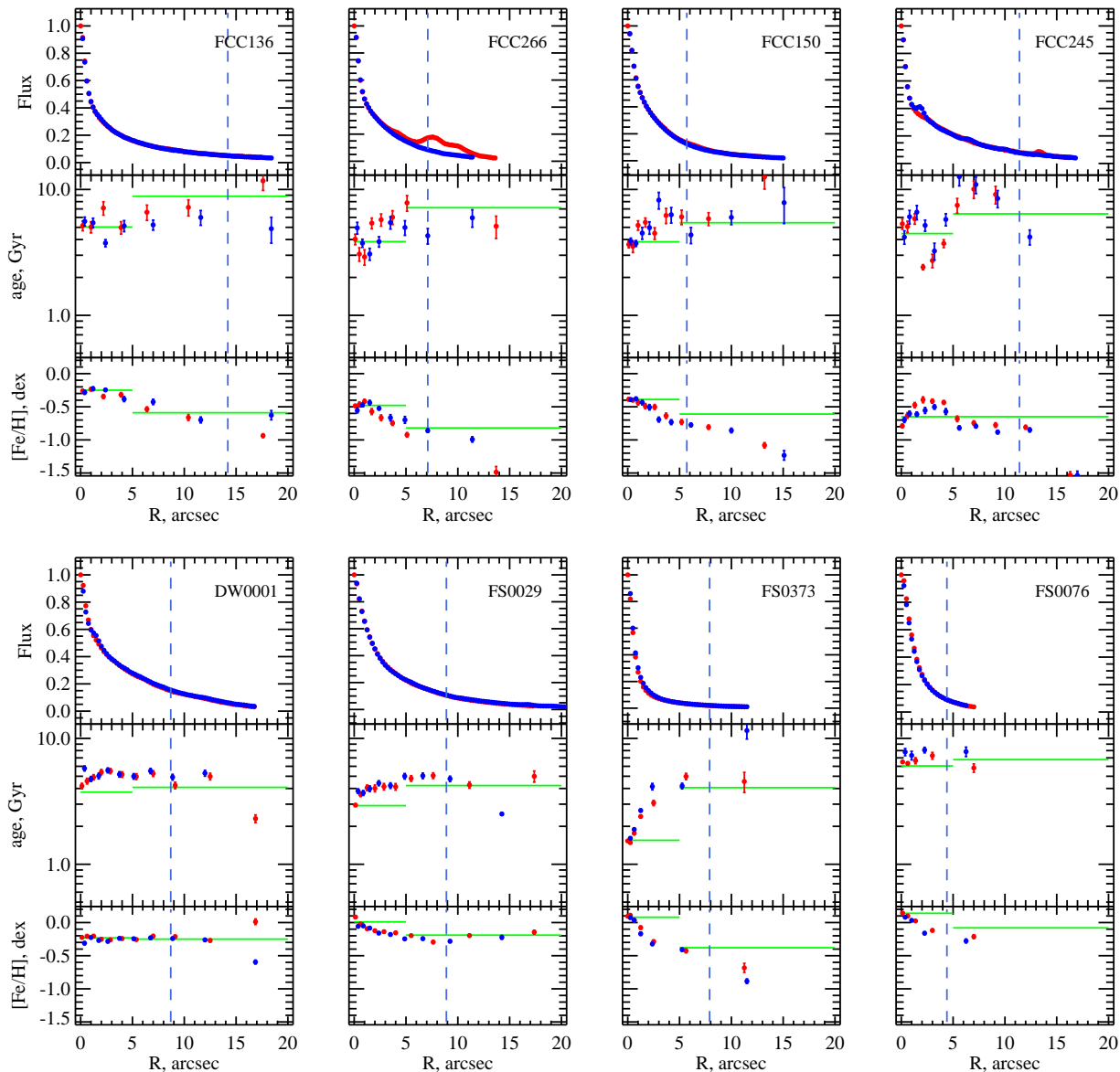


Figure 1. Radial profiles of the dEs with the shortest star-formation time-scale (see paragraph 4.1). In the outer regions we binned the spectra to have $\text{SNR} > 20$. One half-light radius, R_e , is indicated with a vertical blue dashed line. The SSP-equivalent metallicities and ages within the 1 arcsec (uncorrected for line-of-sight contamination) and $1 R_e$ extractions (Sect. 4) are shown with green lines (for readability these lines are arbitrarily drawn from 0 to 5 arcsec and from 5 to 20 arcsec). The profiles are folded around the luminosity peak, the red points are for the ‘right’ side of the centre (North or East), and the blue for the ‘left’.

count for the internal kinematics. A least-square minimization provides the parameters of the population model, age and metallicity in the case of a single stellar population (SSP). The main characteristics of the method, described and validated in Koleva et al. (2008c), is to fit the full spectrum, pixel-by-pixel, while the most common approach uses spectrophotometric indices. The SSP-equivalent ages and metallicity for central extractions of the present data were found perfectly consistent with Lick indices and three times more precise (Michielsen et al. 2007). Beside the precision, another advantage of the method is its insensitivity to the presence of emission lines, that can be either masked or fitted with additive Gaussians.

We are using population models generated with *Pe-gase.HR* (Le Borgne et al. 2004) assuming Salpeter IMF and Padova isochrones and build with the *ELODIE.3.1* library (Prugniel & Soubiran 2001; Prugniel et al. 2007b). These models have a well calibrated line spread function (LSF, i. e. instrumental broadening) of 0.55 \AA corresponding to a resolution $R \approx 10000$ or instrumental velocity dispersion $\sigma_{\text{instr}} = 13 \text{ km s}^{-1}$ at $\lambda = 5500 \text{ \AA}$.

The *ELODIE* library, as any other empirical libraries, consists mostly of stars of the solar neighborhood and therefore presents the abundance pattern of this environment. The chemical composition of the stars is scaled-solar at high metallicity, but becomes enhanced in α -elements at low

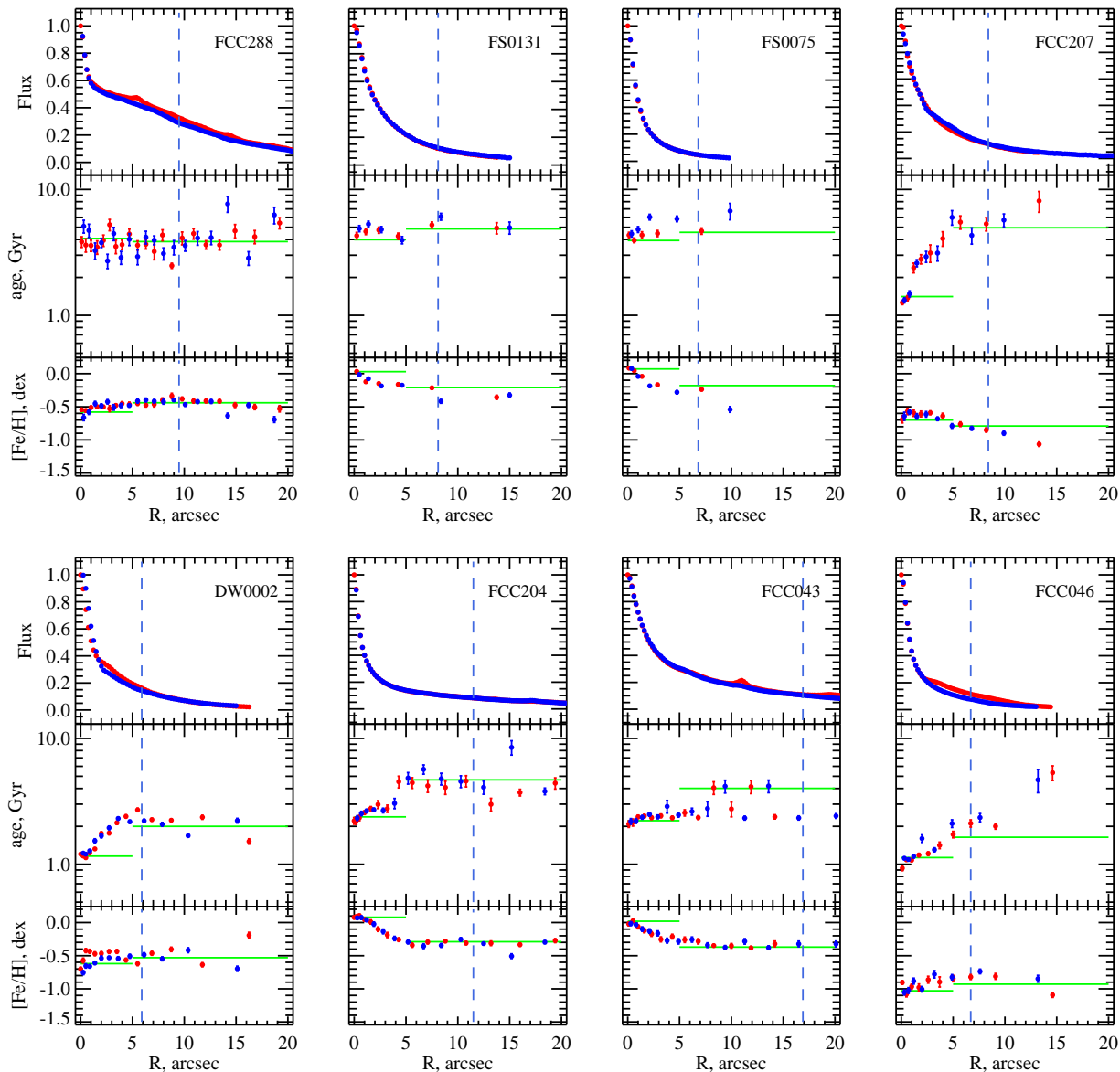


Figure 2. Radial profiles of the dEs with the longest formation time scale (see paragraph 4.1). The symbols are as in Fig. 1.

metallicity ($[\text{Fe}/\text{H}] < -1$). A consequence of this feature is that low metallicity globular clusters ($[\text{Fe}/\text{H}] \approx -2$; $[\text{Mg}/\text{Fe}] \approx 0.3$) are correctly fitted, while for high metallicity clusters ($[\text{Fe}/\text{H}] \approx -0.5$; $[\text{Mg}/\text{Fe}] \approx 0.3$) the models will under-fit the Mg lines. This effect is illustrated in Prugniel et al. (2007a). Models of Lick indices with various α -elements abundances (Thomas et al. 2003b) are commonly used to measure the α -enhancement, and the equivalent has been also explored for spectral models (Koleva et al. 2008a): The empirical models were corrected for the differential effect of the α -enhancement computed in a theoretical library (Coelho et al. 2005). This method proved to be efficient to measure the enhancement of globular clusters and to absorb the residuals on the Mg_b feature. It was also found from Monte-Carlo simulations that the measurements of $[\text{Fe}/\text{H}]$ and $[\text{Mg}/\text{Fe}]$ with full-spectrum fitting are independent. In other words,

a mismatch of $[\text{Mg}/\text{Fe}]$ does not affect the measurement of $[\text{Fe}/\text{H}]$.

Previous studies found that the populations of dEs have close-to-solar $[\text{Mg}/\text{Fe}]$ (Thomas et al. 2003a), and in this luminosity range (similar to NGC 205) the metallicity is around $[\text{Fe}/\text{H}] \approx -0.5$. Therefore, we do not expect an important Mg_b residuals, but possibly a small under-abundance with respect to the library.

As we know that this will not affect the $[\text{Fe}/\text{H}]$ measurements, we preferred to conservatively use the empirical library instead of the α -elements resolved semi-empirical one which is not tested in details. Examination of the residuals of the fits to the dE spectra does not reveal significant residuals on the Mg lines (in most of the cases the residuals in the Mg_b region are inside the 1σ errors).

The analysis is made with the ULYSS¹ package (?). The first step is to reduce the resolution of the models to that of the observations. To do this, we first determine the relative LSF between the observations and the models as a function of the wavelength, and then we convolve the models by the appropriate function (for more details, see Koleva et al. 2008c; ?). The LSF analysis was made using twilight spectra taken with the same setup.

3.2 Radial profiles

The analysis was performed with a SSP model parameterized by its age, metallicity, velocity and velocity dispersion. A multiplicative polynomial of order 20 was included in the model and the outliers were iteratively rejected. Each independent 1D-spectrum was generated by binning together spectra until $S/N=20$ was reached, starting from the central spectrum. The last point has $S/N>10$. The radial profiles for the 16 galaxies are shown in Figs. 1 and 2. For three galaxies, the H_β , H_γ and $[OIII] \lambda 5007\text{\AA}$ emission lines were fitted with gaussians in the same time as all the other free parameters. The error bars, estimated from the noise and quality of the fit, give the independent errors on the age and on the metallicity and do not take into account the age-metallicity degeneracy (a metallicity offset is compensated by a bias of the age): some points are deviating from a smooth profile by more than the error bar, but they lie on the same age-metallicity degeneracy line (or actually age-metallicity- σ surface). The error bars determined from Monte-Carlo simulations are about twice larger, as they take also into account the degeneracies.

The first thing to notice is the high degree of symmetry of the profiles (asymmetries seen in FCC043 and 266 are due to background galaxies along the slit, see Appendix). Most galaxies show significant metallicity gradients, with metallicity declining by 0.5 dex over a distance of one half-light radius, on average, with some exceptions discussed later in this paper.

3.3 Inner 1 arcsec, corrected for line-of-sight contamination

We also study the inner 1 arcsec extraction, corrected for contamination by stars along the line-of-sight that are outside of the inner sphere with 1 arcsec diameter. The procedure is clarified in Fig. 3. The spectrum at a projected radius of 0.5 arcsec is to a good approximation the amount light that is contributed by stars along the line of sight in front of and behind the inner 1 arcsec radius sphere. This means that a fraction

$$\mathcal{F}_{\text{outside } 1 \text{ arcsec}} = \frac{\sum_i F_{1 \text{ arcsec}, \lambda r_i}}{\sum_i F_{i, \lambda r_i}} \quad (4)$$

of the light in the 1 arcsec extraction comes from stars outside the inner 1 arcsec diameter sphere. We fitted SSPs to the corrected 1 arcsec (Table 5). In 6 cases, when the photometric profile is flat, the correction implied a subtraction of a too large fraction of the light, and no correct fit could be obtained.

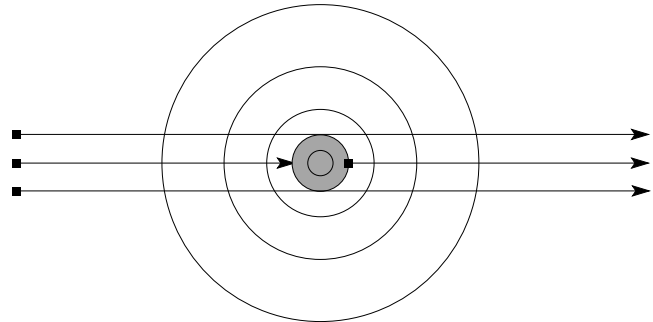


Figure 3. The spectrum at a projected radius of 0.5 arcsec (the upper and lower lines of sight) is to a good approximation the amount of light that is contributed by stars along the line of sight in front of and behind the inner 1 arcsec diameter sphere (the middle line of sight).

In 7 cases out of 10, the population in the core is significantly younger than in the 1 arcsec extraction, by 0.3 to 0.7 dex. The metallicities do not show systematics. The most striking case is FS 29 where the nucleus appears very young and metal-rich.

4 SPATIAL DISTRIBUTION OF THE STAR-FORMATION HISTORIES

The stellar populations of dEs are commonly described by SSP-equivalent ages and metallicities, derived from spectra (Geha et al. 2003; Michielsen et al. 2007). If the population is not co-eval, this is essentially representing the 'light-dominant' epoch of star formation and therefore the derived age and metallicity are often called 'light-weighted' (though this short-cut is not rigorous).

Owing to the high quality of the present spectra, we attempt here to reconstruct more realistic star-formation histories (SFHs).

So far, SFHs of early-type dwarf galaxies have been reconstructed for objects in the Local Group. Thanks to their proximity, high-quality stellar color-magnitude diagrams (CMDs) can be assembled and analysed by fitting synthetic CMDs to the observed ones (Gebell 2000; Dolphin 2002; Dolphin et al. 2003; Cole et al. 2007). Beside the significant old stellar population (age > 8 Gyr) and absence of ongoing star formation, the diversity of recovered SFHs is startling. Some dwarf spheroidals are genuine old stellar systems, with little or no star formation after the initial burst that formed the system (e.g. Ursa Minor, Draco, Sculptor). Others have been forming stars at an almost constant rate until a few Gyr ago (e.g. Carina, Sagittarius, Leo II). Leo I is an example of galaxy with a recent major star formation event, between 3 and 1 Gyr ago, after which the star formation rapidly peters out.

Further than the Local Group the SFH has been determined from integrated light spectra by decomposing an observation onto a SSP basis of three SSPs (Lisker et al. 2006) (1-10 Myr, 10-500 Myr and 5 Gyr) or parametrized by a exponentially declining SFR (Pasquali et al. 2005; in the field dwarf galaxy APPLES 1). In our sample, three galaxies (FCC46 and 207, NGC5898 DW2) show H_β emission

¹ <http://ulyss.univ-lyon1.fr>

Table 5. Results from the SSP fits of the central 1 arcsec, $1R_e$ and the 1 arcsec corrected for the light on the line-of-sight, and light-averaged age and metallicity determined from the star formation histories. The ages are in Gyr and metallicity in dex, relative to the Sun.

NameA	1 arcsec		SSP-equivalent $1R_e$		1 arcsec corrected		Computed from SFH 1 arcsec		$1R_e$	
	age, Gyr	[Fe/H], dex	age, Gyr	[Fe/H], dex	age, Gyr	[Fe/H], dex	age	[Fe/H]	age	[Fe/H]
FCC136	5.03 ± 0.55	-0.25 ± 0.03	8.58 ± 0.71	-0.59 ± 0.03	3.64 ± 2.33	-0.45 ± 0.18	7.0	-0.26	8.8	-0.60
FCC266	3.85 ± 0.30	-0.48 ± 0.03	7.04 ± 0.40	-0.81 ± 0.03	–	–	6.2	-0.36	9.0	-0.85
FCC150	3.84 ± 0.19	-0.39 ± 0.02	5.45 ± 0.27	-0.61 ± 0.03	1.83 ± 2.23	-0.32 ± 0.19	6.5	-0.45	6.3	-0.67
FCC245	4.46 ± 0.64	-0.65 ± 0.04	6.30 ± 0.55	-0.65 ± 0.04	2.84 ± 2.29	-0.76 ± 0.30	5.6	-0.68	8.5	-0.70
DW1	3.74 ± 0.16	-0.23 ± 0.01	4.82 ± 0.10	-0.26 ± 0.01	1.78 ± 1.31	-0.15 ± 0.20	5.3	-0.25	7.1	-0.27
FS29	2.92 ± 0.05	0.01 ± 0.01	4.25 ± 0.08	-0.19 ± 0.01	0.70 ± 0.54	0.46 ± 0.13	4.3	-0.00	5.7	-0.21
FS373	1.55 ± 0.02	0.08 ± 0.01	4.01 ± 0.08	-0.39 ± 0.01	–	–	2.3	0.05	5.8	-0.38
FS76	6.04 ± 0.07	0.14 ± 0.01	6.92 ± 0.21	-0.08 ± 0.01	–	–	6.2	0.13	6.9	-0.06
FCC288	4.08 ± 0.50	-0.58 ± 0.03	3.85 ± 0.12	-0.44 ± 0.01	–	–	6.0	-0.65	4.5	-0.55
FS131	3.99 ± 0.19	0.03 ± 0.01	4.58 ± 0.19	-0.20 ± 0.02	–	–	4.2	0.02	6.5	-0.22
FS75	3.93 ± 0.09	0.07 ± 0.01	4.81 ± 0.15	-0.19 ± 0.01	4.51 ± 1.23	0.16 ± 0.05	4.1	0.09	7.0	-0.23
FCC207	1.41 ± 0.07	-0.70 ± 0.05	4.64 ± 0.15	-0.77 ± 0.02	0.34 ± 1.78	-0.68 ± 0.96	1.8	-0.68	5.0	-0.86
DW2	1.16 ± 0.01	-0.62 ± 0.03	2.08 ± 0.02	-0.56 ± 0.01	0.78 ± 0.28	-1.10 ± 0.16	0.7	-0.44	3.0	-0.69
FCC204	2.38 ± 0.08	0.08 ± 0.02	4.68 ± 0.13	-0.29 ± 0.01	1.50 ± 0.44	0.15 ± 0.07	2.9	0.06	5.2	-0.43
FCC043	2.22 ± 0.07	-0.02 ± 0.02	4.01 ± 0.08	-0.38 ± 0.01	–	–	2.2	-0.01	4.2	-0.47
FCC046	1.13 ± 0.03	-1.03 ± 0.04	1.65 ± 0.05	-0.93 ± 0.04	1.17 ± 0.26	-1.31 ± 0.47	0.2	-0.43	1.8	-0.72

revealing the existence of a weak contemporary star formation activity. (The [OIII] 5007Å emission lines discovered in the fits residuals of other galaxies of the sample: FCC150 and 204, NGC5898 DW1, FS76, 131 and 373, in both the central and half-light radius extractions, are probably due to evolved stars – planetary nebulae and SN remnants).

The diversity of SFHs in the Local Group urges for a generalization of time-resolved analyses.

We will restore the SFH using two independent methods: ULYSS and STECKMAP² (Ocvirk et al. 2006) that we will apply to both the central and the effective radius regions.

4.1 Reconstruction of the star-formation histories

We will use two inversion methods: (i) a decomposition in 3 or 4 SSPs of free age and metallicity using ULYSS and (ii) a regularized decomposition on a basis of SSPs with STECKMAP.

With ULYSS we can fit the observation against a positive linear combination of an arbitrary number of sub-populations, setting some constraints on the age and metallicity of each of them. The advantage of the method is its flexibility and possibility to visualize the parameters space using χ^2 maps along the different projections. The significance of a decomposition can be checked using Monte-Carlo simulations.

As a first approximation to a complex SFH we fitted two burst models, imposing the young population to be younger than 1 Gyr. Often, one of the two components was pushing on this 1 Gyr age limit, indicating that the other box dominates the light and can probably be resolved at a higher time resolution.

This drove us to approximate the SFH by three SSPs. In order to maintain the degree of freedom at the minimum,

we initially fixed the age of the oldest burst to 12 Gyr. And we chose the acceptable limits of the two other bursts as:

(i) Young population aged between 12 and 800 Myr and with metallicities between -1.0 and 0.69 dex (note though that the SSP models are probably not very reliable for ages below 50 Myr and too high metallicities);

(ii) Intermediate population aged between 0.8 and 5 Gyr and with metallicities between -1.0 and 0.4 dex.

The old population has a metallicity bounded between -2.3 and -0.4 dex.

This 3-populations fit is in general satisfactory in the sense that the χ^2 is significantly lower than for the SSP fit and that the episodes are well within their assigned bounds in ages and metallicity.

In some cases however one component appears to be below the 3σ detection limit or to reach an age-limit of the box. In the first case we exclude this component and in the second we merge it with the neighbouring one. The results are in Table. 6 and the distributions of the light fractions in the different components for the two aperture extractions are shown on Fig. 6. For two galaxies, FCC046 and NGC5898 DW2, where a very young population is detected, we fitted 4 bursts to resolve the lowest age bin. The results are in Table 7.

We detect an important old component (over 10 Gyr) in all galaxies except FS 76 (in FS75 and 131 the old population is detected only in the outer extraction), and a young population (< 1 Gyr) in 8 galaxies: FCC150, DW1, FS373, FCC288, FCC207, NGC5898 DW2, FCC204, FCC46. The young population is generally more concentrated than the oldest components (Fig. 6).

To investigate the relation between the SFH and the other characteristics, we ordered the galaxies according to the mass fraction contained in the old population (averaged between the two extractions), as it gives an idea of the formation time-scale. Tables 1, 5, 6 and Fig. 1, 2, 4 and 5 are sorted in this order.

This SFH reconstruction with ULYSS allowed to test

² http://astro.u-strasbg.fr/Obs/GALAXIES/stecmap_eng.html

Name	Extraction	age, Gyr	[Fe/H]	Fraction, %	age, Gyr	[Fe/H]	Fraction, %	age, Gyr	[Fe/H]	Fraction, %
FCC136	1arcsec				1.03±0.19	0.50±0.14	21.77±1.39	12.00(fixed)	-0.48±0.05	78.23±1.39
FCC136	1Re							8.28±1.16	-0.58±0.04	100.00
FCC266	1arcsec				2.59±0.14	0.01±0.09	52.72±1.55	12.00(fixed)	-1.19±0.14	47.28±1.55
FCC266	1Re				3.60±1.81	0.28±0.38	20.02±0.63	12.00(fixed)	-1.20±0.16	79.98±0.63
FCC150	1arcsec				3.34±1.35	-0.22±0.15	72.59±1.21	12.00(fixed)	-1.18±0.64	27.41±1.21
FCC150	1Re	0.10±0.01	0.16±0.22	2.77±0.06	4.99±0.00	-0.12±0.02	53.68±0.14	12.00(fixed)	-1.47±0.04	43.54±0.19
FCC245	1arcsec				2.63±0.22	-0.11±0.09	54.74±1.38	12.00(fixed)	-1.52±0.19	45.26±1.38
FCC245	1Re				1.99±0.91	0.40±0.29	20.95±1.23	12.00(fixed)	-0.98±0.11	79.05±1.24
DW1	1arcsec				1.06±0.12	0.10±0.12	27.71±0.48	12.00(fixed)	-0.42±0.03	72.29±0.48
DW1	1Re	0.38±0.11	0.40±0.26	9.11±0.25	4.24±1.23	0.70±-0.00	10.64±0.40	12.00(fixed)	-0.57±0.03	80.24±0.61
FS29	1arcsec				2.56±0.29	0.20±0.06	67.83±1.34	12.00(fixed)	-0.54±0.12	32.17±1.34
FS29	1Re				0.91±0.07	0.49±0.05	24.13±0.33	12.00(fixed)	-0.45±0.02	75.87±0.34
FS373	1arcsec	0.41±0.03	0.59±0.05	25.60±0.36	2.80±0.15	-0.11±0.03	74.40±0.23	12.00(fixed)	-2.16±0.22	
FS373	1Re	0.80±-0.00	0.32±0.13	22.33±1.17	1.43±0.90	-2.23±0.45	7.10±0.54	12.00(fixed)	-0.57±0.04	70.56±0.71
FS76	1arcsec							6.54±0.09	0.11±0.01	100.00
FS76	1Re							7.46±0.28	-0.10±0.01	100.00
FCC288	1arcsec				2.68±0.20	-0.06±0.09	53.92±1.36	12.00(fixed)	-1.41±0.18	46.08±1.36
FCC288	1Re	0.51±0.18	0.29±0.38	8.05±0.37	1.15±0.21	0.37±0.14	20.84±1.00	12.00(fixed)	-0.78±0.03	71.11±0.81
FS131	1arcsec				4.32±0.33	0.03±0.02	100.00			
FS131	1Re				4.53±0.27	-0.18±0.03	99.87±0.40	12.00(fixed)	-2.25±0.18	0.13±0.40
FS75	1arcsec				4.26±0.17	0.07±0.01	100.00			
FS75	1Re				1.76±0.13	0.58±0.05	28.16±0.72	12.00(fixed)	-0.59±0.04	71.84±0.72
FCC207	1arcsec	0.24±0.14	0.70±0.24	17.51±1.30	1.80±0.97	-0.20±0.38	44.01±1.65	12.00(fixed)	-2.20±0.33	38.48±2.33
FCC207	1Re				3.40±1.36	-0.34±0.22	57.83±1.25	12.00(fixed)	-1.60±0.31	42.17±1.25
DW2	1Re	0.54±0.05	0.48±0.07	18.45±0.44	3.10±0.48	-0.60±0.10	62.43±0.23	12.00(fixed)	-2.27±0.23	19.12±0.47
FCC204	1arcsec				2.42±0.09	0.14±0.03	93.12±0.54	12.00(fixed)	-2.22±0.23	6.88±0.54
FCC204	1Re	0.01±0.00	-2.30±0.00	1.31±0.24	5.00±0.00	-0.02±0.04	73.16±0.58	12.00(fixed)	-1.73±0.16	25.53±0.77
FCC043	1arcsec				2.24±0.07	-0.02±0.02	100.00			
FCC043	1Re				2.76±0.04	-0.04±0.03	71.31±0.38	12.00(fixed)	-1.55±0.11	28.69±0.38

Table 6. Population histories of the dEs, reconstructed from three episodes of star formation. In the first column is the name of the galaxy and its extractions, the second is for the χ^2 -s, followed by the age (in Gyr), [Fe/H] (in dex) and light fraction for the young (from 0-0.8Gyr), intermediate (from 0.8 to 5 Gyr) and old (\sim 12 Gyr) populations.

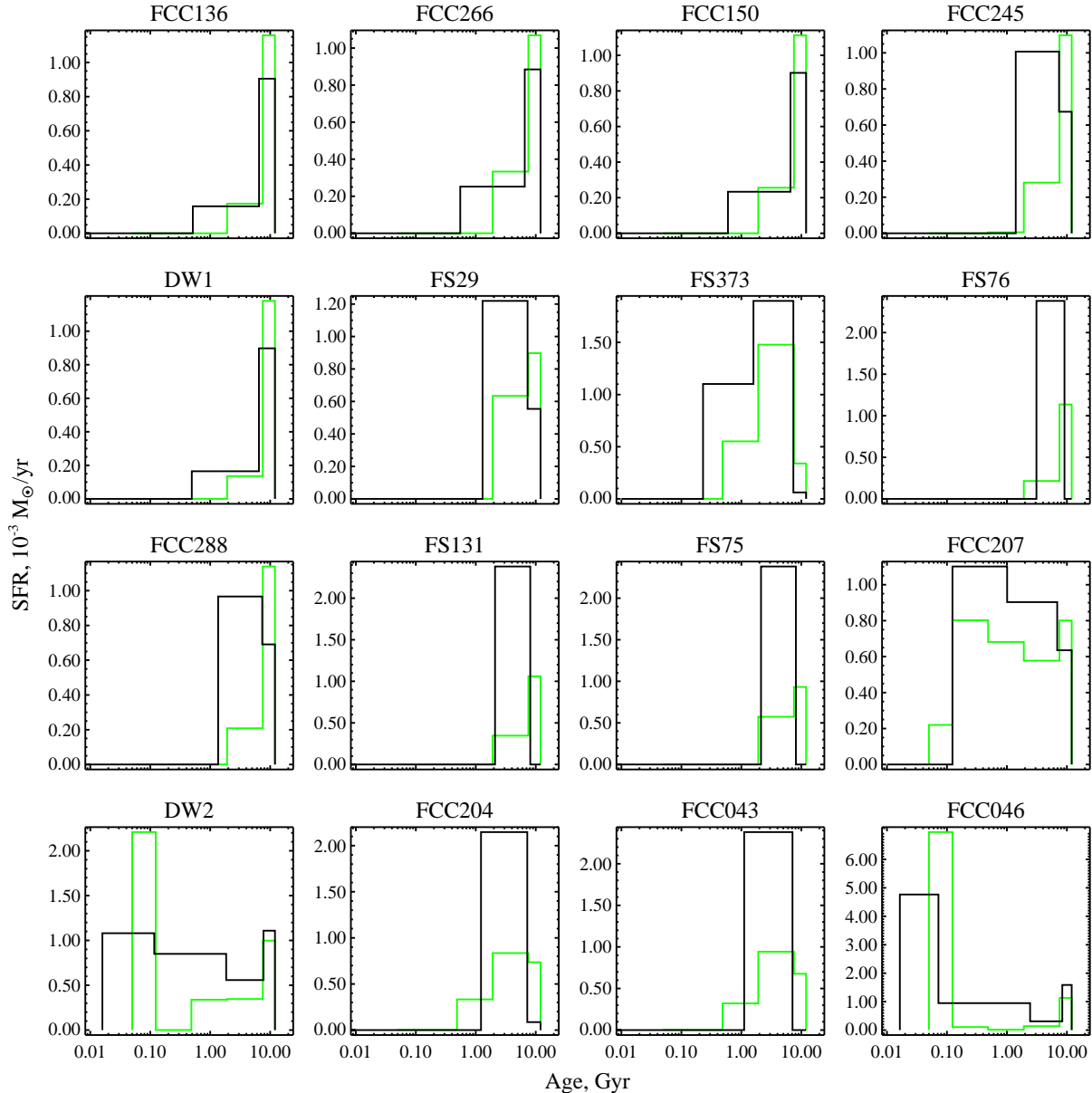


Figure 4. SFR (black for STECKMAP, green for ULYSS) for the inner arcsec of the dEs (with assumed mass of $10^7 M_{\odot}$.)

step-by-step different hypotheses (choice of the number of bursts and of their age distribution, significance of each burst) and we gained confidence in the relevance of the results. But seeking for a more objective and automatic method, we face the known difficulty of the instability of this inversion. Several methods were devised to cope with this situation: Moultaqa (2005), STARLIGHT³ (Cid Fernandes et al. 2005), MOPED (Heavens et al. 2000), STECKMAP and more recently VESPA (Tojeiro et al. 2007).

We analysed the sample with STECKMAP, using the same population models (Pegase.HR with Elodie 3.1) and choosing a resolution into 5 age bins. Any number of age

bins can be required with STECKMAP, and the program determines the SFH with the a priori that it should be smooth. As we have shown that our 3 or 4 SSPs decomposition is realistic, we chose to use STECKMAP with 5 age boxes logarithmically spaced. These fixed-limits boxes give a resolution comparable to the ULYSS fits.

The SFR is represented in Fig. 4 and 5 as a function of time for both the ULYSS (in black) and STECKMAP (in green) fits for the 1 arcsec and 1 Re extractions. The spectral analysis does not provide immediately the SFR, but rather give the optimal weight of the different SSP components. To derive the SFR we have to assume that these individual SSPs approximate in fact the SFH over a period of time, and the simplest is to consider that the SFR is constant in each box. Then one has to choose the limits of these boxes. Setting the

³ <http://www.starlight.ufsc.br/>

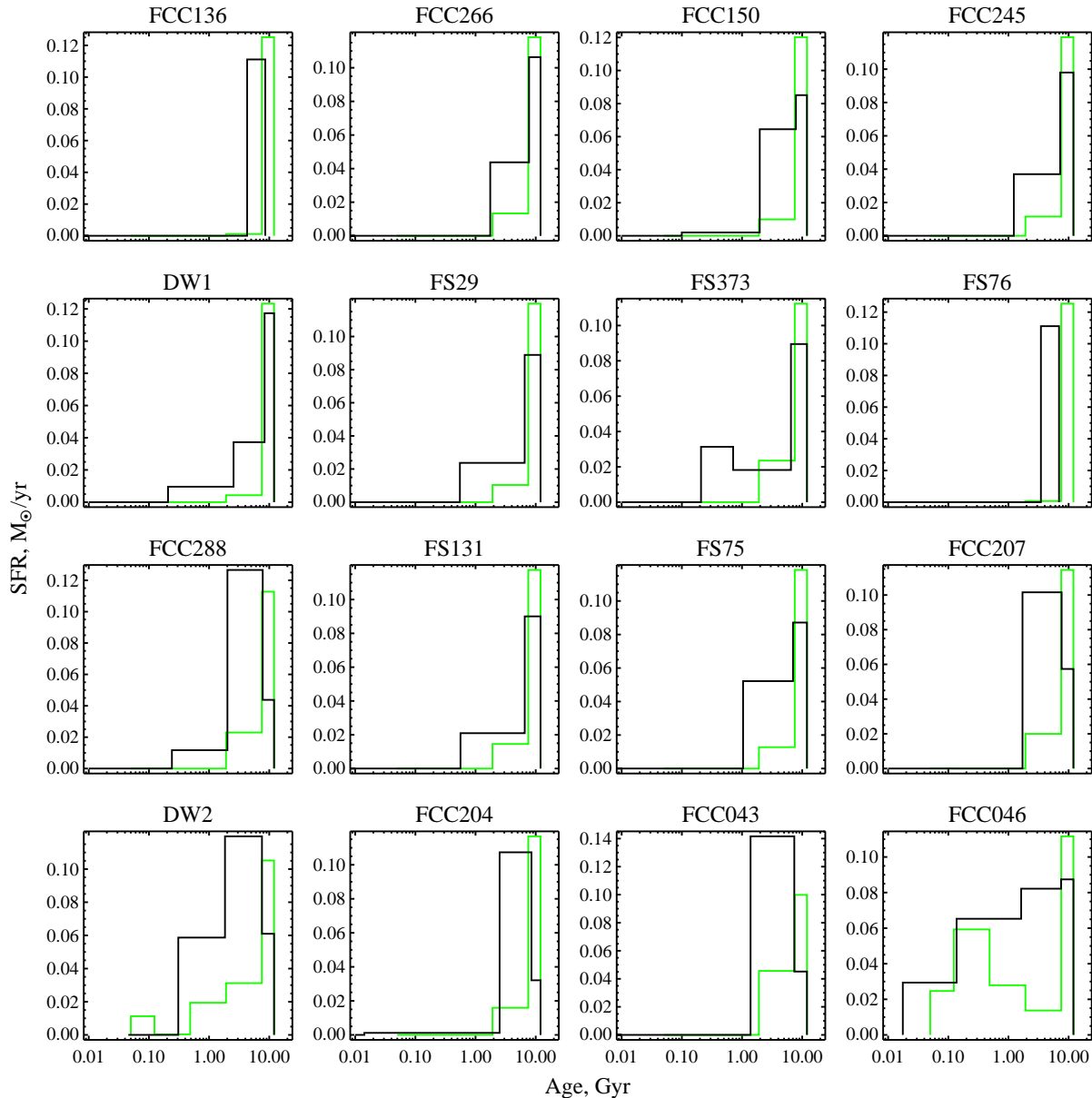


Figure 5. SFR (black for STECKMAP, green for ULYSS) for the inner $1R_e$ of the dEs (with assumed mass of $10^9 M_\odot$).

limits at medium location between the ages (or more properly their logarithm) of the components, and deriving the outer limits such that the age of the extreme components sit in the middle of their boxes, is the first idea. However, one has to realize that the size of the older box, which is the longer, is not really constrained by the data. The only physical constraint is that the initial burst lasted at least one Gyr, otherwise $[\text{Mg}/\text{Fe}]$ would have been enhanced, but we are free to consider a width between a couple of Gyr and about 6 Gyr (from 8 to 14 Gyr). This implies an uncertainty by a factor 3 on the initial SFR. We chose to fix the beginning of the star-formation at 14 Gyr in the past, therefore the reported initial SFR is a lower limit of the mean SFR during the first Gyr of the galaxy. It is likely that during this period the SFR passed through a succession of more violent

episodes. The choice of the lower limit of the most recent box is less critical, and because of the exponential decrease of the luminosity of a population, we set the limit of the first box to the age of the first SSP.

These assumptions have to be taken into account when reading Fig. 4 and 5, but at least these figures allow a direct comparison of the histories reconstructed with both methods.

4.2 Reliability of the determined star formation histories

Constraining the star formation histories is a considerably harder task than fitting SSPs, and it is legitimate to ques-

Table 8. Population histories of the dEs, from Monte-Carlo simulations. Same caption as Table 6.

Name	Extraction	age, Gyr	[Fe/H]	Fraction, %	age, Gyr	[Fe/H]	Fraction, %	age, Gyr	[Fe/H]	Fraction, %
FCC136	1arcsec				1.50±1.22	0.46±0.22	27.28±17.90	12.00(fixed)	-0.60±0.34	72.72±17.90
FCC136	1Re				8.57±1.12	-0.59±0.03	100.00			
FCC266	1arcsec				1.98±0.98	0.16±0.30	45.39±21.31	12.00(fixed)	-1.18±0.40	54.61±21.31
FCC266	1Re				2.96±1.10	0.21±0.25	23.80±11.51	12.00(fixed)	-1.19±0.15	76.20±11.51
FCC150	1arcsec				2.04±1.12	0.09±0.32	49.22±28.23	12.00(fixed)	-1.00±0.48	50.78±28.23
FCC150	1Re	0.15±0.11	0.04±0.53	2.76±2.24	3.10±1.32	0.05±0.24	37.65±19.83	12.00(fixed)	-1.18±0.38	59.59±18.42
FCC245	1arcsec				2.97±1.07	-0.09±0.26	53.99±16.51	12.00(fixed)	-1.64±0.35	46.01±16.51
FCC245	1Re				2.10±0.85	0.36±0.14	22.18±6.91	12.00(fixed)	-0.97±0.10	77.82±6.91
DW1	1arcsec				1.37±1.08	0.22±0.23	36.11±26.52	12.00(fixed)	-0.56±0.42	63.89±26.52
DW1	1Re	0.41±0.03	0.61±0.12	7.59±0.87	4.12±0.99	0.42±0.13	20.73±4.13	12.00(fixed)	-0.63±0.05	71.67±4.04
FS29	1arcsec				2.00±0.60	0.31±0.12	56.11±13.49	12.00(fixed)	-0.50±0.19	43.89±13.49
FS29	1Re				1.05±0.04	0.46±0.02	27.47±1.11	12.00(fixed)	-0.47±0.01	72.53±1.11
FS373	1arcsec	0.44±0.04	0.54±0.04	23.92±4.94	2.48±0.95	0.02±0.22	63.33±13.68	12.00(fixed)	-0.74±0.42	12.75±17.52
FS373	1Re	0.49±0.27	0.19±0.42	12.75±7.98	3.40±2.20	0.01±0.25	28.92±8.56	12.00(fixed)	-0.74±0.07	58.33±13.33
FS76	1arcsec				6.20±0.08	0.13±0.01	100.00			
FS76	1Re				6.91±0.09	-0.08±0.01	100.00			
FCC288	1arcsec				2.64±0.86	-0.01±0.32	52.31±18.94	12.00(fixed)	-1.48±0.38	47.69±18.94
FCC288	1Re	0.47±0.09	0.56±0.11	4.64±2.28	1.14±0.04	0.36±0.03	20.49±3.40	12.00(fixed)	-0.73±0.02	74.87±1.58
FS131	1arcsec				4.16±0.27	0.02±0.01	100.00			
FS131	1Re				1.11±0.03	0.38±0.03	26.41±0.93	12.00(fixed)	-0.45±0.02	73.59±0.93
FS75	1arcsec				4.25±0.10	0.06±0.01	100.00			
FS75	1Re				1.76±0.31	0.53±0.04	30.01±2.58	12.00(fixed)	-0.56±0.06	69.99±2.58
FCC207	1arcsec	0.39±0.31	-0.14±0.67	0.03±0.20	2.61±1.48	-0.27±0.57		12.00(fixed)	-0.77±0.03	99.97±0.20
FCC207	1Re				0.63±1.26	-0.86±0.15	21.00±14.57	12.00(fixed)	-0.82±0.07	79.00±14.57
DW2	1arcsec	0.02±0.00	-0.98±0.04	18.53±1.82	0.23±0.02	0.43±0.04	38.17±1.80	2.81±1.60	-0.04±0.33	14.15±8.44
DW2	1Re	0.55±0.03	0.36±0.02	12.53±0.53	3.08±0.03	-0.56±0.01	69.41±0.83	12.00(fixed)	-2.30±0.00	18.07±1.01
FCC204	1arcsec				1.90±0.39	0.27±0.09	84.86±11.53	12.00(fixed)	-0.61±0.28	15.14±11.53
FCC204	1Re	0.11±0.07	0.69±0.00	5.36±1.68	3.31±0.88	0.16±0.15	45.90±14.41	12.00(fixed)	-0.78±0.15	48.73±14.56
FCC043	1arcsec				2.21±0.06	0.04±0.01	100.00			
FCC043	1Re				2.40±0.27	-0.01±0.08	69.56±9.15	12.00(fixed)	-1.24±0.31	30.44±9.15
FCC046	1arcsec	0.02±0.02	0.01±0.04	32.02±8.66	0.13±0.05	0.12±0.11	40.15±8.78	3.91±1.35	-0.42±0.40	7.58±4.54
FCC046	1Re	0.04±0.03	-0.15±0.43	7.79±5.15	0.32±0.16	0.36±0.19	24.84±8.64	2.56±1.06	-0.57±0.52	36.87±18.68

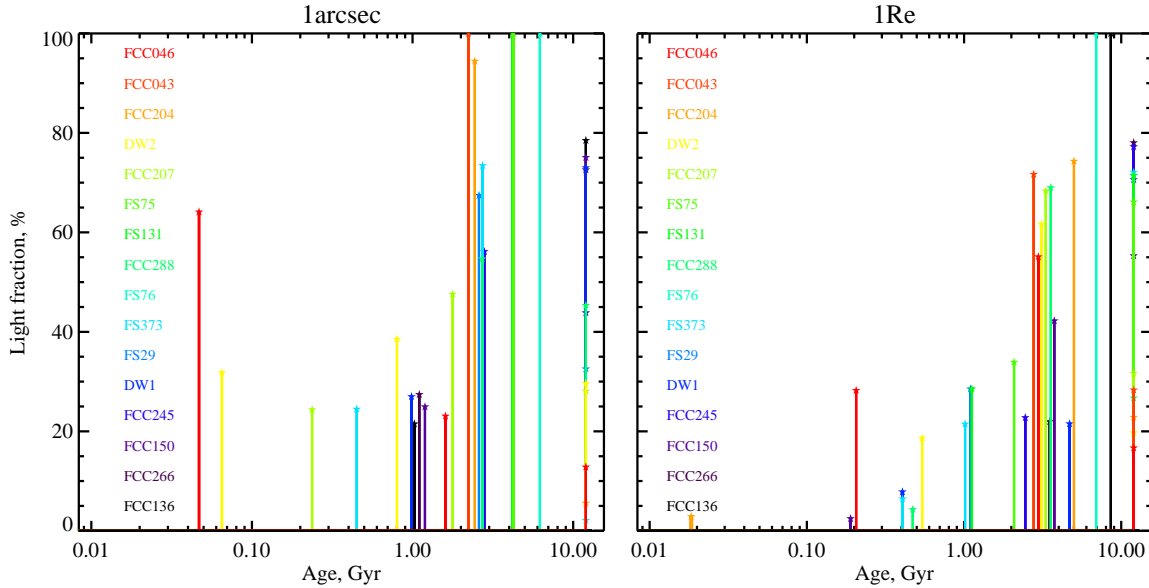


Figure 6. Light fractions of each burst for all the galaxies. Each galaxy is represented with a different color indicated in the frame. Each star formation burst is shown as a vertical bar whose position is its age and height its light contribution to the total spectrum.

Table 7. Four-epochs star formation history for the two ‘young’ galaxies FCC046 and NGC5898 DW2. The light is the light fraction in per cent, ages are in Gyr and metallicity in dex, relative to the Sun.

Burst	FCC046		NGC5898 DW2
	1 arcsec	1 R_e	1 arcsec
1			
light	32±1	5±1	17.5±0.5
Age	0.016±0.001	0.02±0.02	0.015±0.03
[Fe/H]	0.00±0.17	0.0±0.5	-0.8±0.3
2			
light	40±1	29±1	38±1
Age	0.13±0.03	0.26±0.08	0.22±0.02
[Fe/H]	0.13±0.13	0.3±0.2	0.44±0.05
3			
light	7.5±1.2	43±2	18±1
Age	4.7±2.0	2.9±1.4	3.5±0.8
[Fe/H]	-0.7±0.5	-0.8±0.3	-0.1±0.2
4			
light	20±2	22±2	27±1
Age	12	12	12
[Fe/H]	-2.3±0.4	-1.8±0.4	-1.7±0.1

tion the validity of the solutions. Adding degrees of freedom by adjusting a combination of SSPs is likely to reduce the χ^2 , but this does not warrant the correctness of the decomposition.

Multiple local χ^2 minima may appear, and they may not be significantly distinguishable, in the sense that changing the noise realization, the wavelength range or some systematic defects in the model or in the observation, may lead to another solution. If these various solutions are close this will not question the validity of the reconstruction, but it may not be the case. Some solutions may be a posteriori rejected on the basis of physical arguments, but rather than adding this additional layer, the inversion programs regularize the

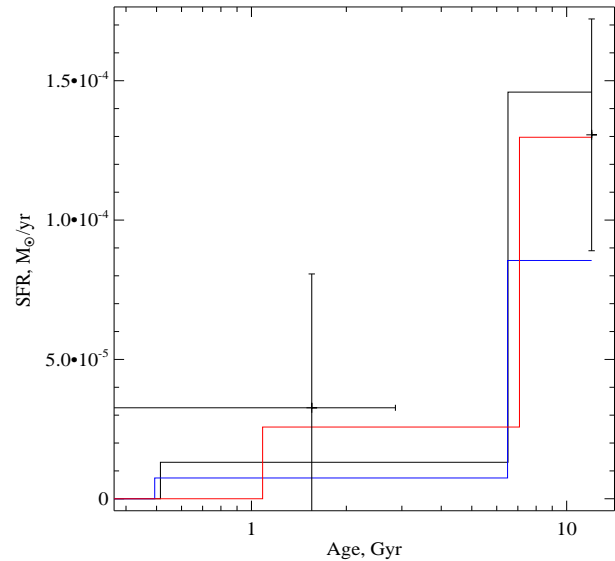


Figure 7. Reliability tests of the SFH of the inner one arcsecond in FCC136 taken as an example: SFR vs. time recovered with ULYSS. The black line is the reference SFH determined with Pegase.HR/Elodie3.1 models using Salpeter IMF (direct solution). The crosses are the Monte-Carlo solution. The red line represents the solution with Vazdekis/Miles grid of models, and the blue with Pegase.HR/Elodie3.1/Kroupa IMF models.

solution by adding constraints. STECKMAP imposes a smooth relation between the metallicity and the age of the components. With ULYSS we decomposed the history in a small number of epochs represented by SSPs (3 or 4 bursts).

The consistency between the two approaches (See Figs. 4 and 5) gives some confidence in the results. And to go further, we are testing below the robustness of the solution with respect to the noise with the help of Monte-Carlo

simulations, and we are considering other physical causes that may alter the solution : (i) the sensitivity to the population model, (ii) the the IMF and (iii) the presence of a blue horizontal branch.

4.2.1 Stability with respect to the noise

One of the basic tests is to make Monte-Carlo simulations with an added noise equivalent to the estimated noise. In the present case, the noise is considered gaussian, with a dependence between the pixels due to the rebinning.

We performed 200 simulations for each galaxy and both extractions. Each time a different random noise realisation is added and the inversion is made. Table 8 gives the average and the dispersion of the measured parameters; they can be compared with the results of the direct fit given in Table 6.

While the error bars of the direct fit ignore the degeneracies between the parameters, the Monte-Carlo simulations take them into account. The most affected from degeneracies parameter is the fraction, while the direct fit gives a precision of 1 per cent, the Monte Carlo simulations show much less confidence (≈ 20 per cent). For the other parameters, this effect of booming the errors is smaller, ≈ 5 times for the ages (from few hundreds Myr up to 1 Gyr) and around two times for the metallicities. The Monte-Carlo estimated values of the parameters are consistent with the direct fit within the error bars.

As an example, in Fig. 7 the Monte-Carlo solution is plotted over the direct solution for FCC 136 in the 1 arcsec extraction.

4.2.2 Sensitivity to the population model

Koleva et al. (2008c) compared SSPs models from Pe-gase.HR/Elodie with models from Vazdekis built with the Miles library⁴ (VazMiles). They found a very satisfactory agreement, despite the fact that the two models use independent ingredients.

We repeated the analysis using VazMiles instead of Pe-gase.HR/Elodie. The result for FCC 207 is shown on Fig. 7. The agreement with the original fit is satisfactory.

4.2.3 Sensitivity to the IMF

The initial mass function of the stars is one of the ingredients of the population model that is not constrained by the observations. We may wonder if it is possible that the detection of an important old (12 Gyr) component, though physically reasonable, is not biased by the assumed IMF. It is probably possible to build an ad hoc IMF to mimic the old component, but this would lack physical support.

In Fig. 7 we are showing the effect of changing the adopted Salpeter's IMF for Kroupa's (Kroupa et al. 1993). Though the choice of the IMF may have a dramatic effect on the mass-to-light ratio, the considered alternative does not affect the SFH.

4.2.4 Sensitivity to a blue horizontal branch

An important effect can be due to extended blue horizontal branches or to blue stragglers which are not represented in the models. Koleva et al. (2008c) have shown that this leads to underestimated ages or mimics a young sub-population in Galactic globular clusters, as also suggested by Li & Han (2008). In the Local Group, Mapelli et al. (2007) detected blue stragglers.

However, compared to the effect seen in Koleva et al. (2008c), where the excess of blue stars was seen as a small and well detached young component, the SFH presented here are considerably more time resolved. So, we believe that the possible presence of blue stragglers cannot be an important explanation for the extended SFH.

After this series of tests, we are reasonably confident in the reliability of the reconstructed SFH.

5 DISCUSSION

The main features standing out from our analysis are the large diversity of the zoo of SFHs and of the radial gradients of SSP-equivalent age and metallicity.

In this section we will discuss the radial gradients detected in the populations (5.1) and the star formation history (5.2). Then we will have a close look at the central region (5.3) and we will critically review the hypothesis concerning the origin of the dEs (5.4).

Our sample is too small to draw any firm conclusions about the connection between the environment and the population parameters. However, these data do not suggests such a connection. It naturally does not imply that the environment is not a key factor controlling the evolution.

5.1 Radial gradients of the stellar populations

Many of the observed dEs show a radially increasing age. The extremes are formed by FCC288 (dS0(7),N), FS76 (dE1), FS131 (dE5,N), and NGC5898 DW1 (dE3), which show almost no age gradient, on the one hand, and FCC207 (dE2,N) and FCC046 (dE4,N) which show an age gradient of over 5 Gyr between the centre and $2R_e$, on the other.

Most galaxies (10/16) also show significant metallicity gradients, with metallicity declining by 0.5 dex over a distance of one half-light radius, on average. This is comparable to what has been found for the Local Group dE NGC 205 (-0.6 ± 0.1 dex/ R_e , Koleva 2009). The exceptions to this pattern are discussed below. We note that the age and metallicity opposite gradients conspire to reduce the color gradients that may be observed.

5.1.1 Flat metallicity profiles

The galaxies standing out from the strong metallicity gradient rule are FCC288 (dS0(7)), FCC204 (dS0(6),N), NGC5898 DW2 (dE6), and FS29 (dE5), which, outside of the inner few arcseconds, have essentially flat metallicity profiles out to the last data point. For instance, FS29 and FCC204 have a metallicity gradient in the centre, but the profile flattens out beyond $0.5 R_e$. The first four galaxies

in this list have the common property of being significantly flattened and fast rotating. FCC288 and FCC204 contain clear evidence for embedded stellar discs (De Rijcke et al. 2003a). NGC5898 DW1 (dE3) and FCC046 (dE4,N) have flat metallicity profiles although they are somewhat rounder objects. However, like FCC204 and FCC288, NGC5898 DW1 has a positive C_4 coefficient which indicates that it has discy isophotes (deviations of the isophotes from a pure elliptic shape are quantified by expanding the intensity variation along an isophotal ellipse in a fourth order Fourier series; C_4 measures the disciness/boxiness of the isophotes, see e.g. De Rijcke et al. (2003a)). Also, its flattening is much stronger in the inner $10''$ ($\epsilon \sim 0.5$) then in the outer parts of the galaxy ($\epsilon \sim 0.2$). In the terminology of Lisker et al. (2007), FCC204, FCC288, and NGC5898 DW1 would be classified as dE(di) objects. Beside their morphology and flat metallicity profile, the dE(di) galaxies do not share other properties. They span the whole range of age, metallicity or formation time-scale of the sample and are not found preferentially in either cluster or group environments.

The spatial chemical homogeneity in their stellar population properties is reminiscent of the dwarf irregular galaxies (dIrrs): See e.g. Lee et al. (2006) and references therein for a discussion of the non-detection of a radial gradient in the stellar and nebular abundances measured in NGC6822 and in other dIrrs. There, supernova feedback is expected to expell hot enriched gas which, after a delay of over 10^8 yr, rains back onto the galaxy's stellar disc (Mac Low & Ferrara 1999; Rieschick & Hensler 2003). This similarity between dIrrs and dE(di)s could therefore be interpreted as another evidence for an evolutionary link between these two types of dwarfs.

5.1.2 Strong metallicity gradients

Strong metallicity gradients are observed in 10 out of 16 dEs. In some Local Group dwarf spheroidals, such as the Sagittarius dwarf (Alard 2001) and the Fornax dwarf (Battaglia et al. 2006) the gradients are due to the imposition of populations of different ages and metallicities. The younger and more metallic populations being more centrally concentrated, the combined population displays a negative metallicity gradient and a positive age gradient. According to this formation scenario, one would expect the metallicity gradient to build up over time. If the present sample can be considered as representative of an homogeneous family whose variety is due to the time elapsed since the last star formation event, we would expect to see the strongest gradients in the objects with the youngest SSP-equivalent ages. This effect is clearly not seen. This mostly says that the sample is not a simple mono-variate family.

The metallicity gradients are also detected when we compare the 1 arcsec and $1 R_e$ extractions, either through their SSP-equivalent characteristics (Table 5) or through their light-averaged description computed from the SFH reconstruction given in Table 6. In Table 9, we give these latter gradients and their values estimated after 3 Gyr of passive evolution (aging of the stars, no kinematical mixing). The gradients are naturally on average smaller than measured on the profiles since the light is integrated in a large aperture. The average age gradient from the observations is 0.26 ± 0.23 and after 3 Gyr vanishes to 0.06 ± 0.11 .

Table 9. Luminosity weighted age and Metallicity gradients. Col. 1: $\log_{10}(\text{Age}_{1R_e}/\text{Age}_{1 \text{ arcsec}})$; Col. 2: $[\text{Fe}/\text{H}]_{1R_e} - [\text{Fe}/\text{H}]_{1 \text{ arcsec}}$; Col. 3 & 4: Same as 1 & 2 after 3 Gyr of passive evolution; Col. 5 & 6: SSP-equivalent gradients computed from Table 5 The more uncertain values are noted with a colon.

Name	Observed: T_0		$T_0 + 3$ Gyr		SSP-equivalent	
	Age	[Fe/H]	Age	[Fe/H]	Age	[Fe/H]
FCC136	0.11	-0.35	-0.06	-0.20	0.23	-0.34
FCC266	0.19	-0.52	0.03	-0.45	0.26	-0.33
FCC150	0.32	-0.61	0.05	-0.38	0.15	-0.21
FCC245	0.18	-0.02	0.09	0.05	0.15	0.00
DW1 ^a	0.13	-0.01	0.13	-0.08	0.11	-0.03
FS029 ^a	0.11	-0.20	0.05	-0.21	0.16	-0.20
FS373	0.41	-0.44	0.12	-0.31	0.41	-0.47
FS076	0.05	-0.19	0.03	-0.19	0.06	-0.22
FCC288 ^a	-0.12	0.09	-0.11	0.10	-0.03	0.14
FS131	0.18	-0.24	0.27	-0.37	0.06	-0.23
FS075	0.23	-0.32	0.24	-0.47	0.09	-0.26
FCC207	0.44	-0.18	0.02:	0.40:	0.52	-0.07
DW2	0.54	-0.21	-0.11:	0.24:	0.25	0.06
FCC204 ^a	0.24	-0.47	0.07	-0.41	0.29	-0.37
FCC043	0.28	-0.46	0.22	-0.65	0.26	-0.36
FCC046 ^a	0.97	-0.33	-0.02:	0.26:	0.16	0.10

^a Flat metallicity profile dE(di) objects.

The mean metallicity gradient evolves from -0.28 ± 0.19 to -0.16 ± 0.30 (the dispersion can be reduced by removing the objects with young populations for which the characteristics of the old populations are more uncertain, and by excluding the dE(di) galaxies discussed above. This experiment, though the important uncertainties, establishes that only 1/3 of the observed mean gradient is due to the light contribution of the younger and more concentrated population. This does not explain the whole gradient which hence appear to be a genuine chemical abundance effect.

Such gradients metallicity are likely to occur if the star formation, initially spread over all the galaxy, gradually becomes more centrally concentrated, together with the increase of the metallicity of the gas. This is shown in SPH simulations (Marcolini et al. 2008; Valcke et al. 2008). The self-regulation of the star formation by the feed-back results in quasi-periodic bursts ('breathing' scenario, Pelupessy et al. 2004; Stinson et al. 2007). The fact that these gradients are seen in the old population (mean gradient 0.3 ± 0.4) indicates that this should have occurred during the few Gyr of the initial formation when 60-90 per cent of the stellar mass formed. The persistence of these gradients over all the live of the galaxies implies that the population has not been mixed, i. e. that the galaxy did not undergo a violent relaxation (after a close encounter or tidal harassment) and also sets constrains on the internal dynamics (the orbits do not mix the population over a large range of radii).

5.2 Star formation histories

The detection of young population and even of ongoing star formation is consistent with the findings of Lisker et al. (2006) who found blue cores in 4 to 5 per cent of a sample of about 450 dEs from the Virgo cluster. We show here

that the late star formation is concentrated (Fig. 6) but still affects the bulk of the galaxy, giving rise to age gradients (Fig. 1 & 2). The mass fraction of the stars formed in the last 5–6 Gyr is typically around 10 per cent.

Does this late star formation need the supply from a reservoir of primordial gas, or can it be fueled by the winds of evolved stars as it may be the case in NGC205 (Davidge 2005) or NGC185 (Martínez-Delgado et al. 1999). According to the population model that we are using (Salpeter IMF), the old population returned 1/3 of its stellar mass to the ISM. Obviously, for the galaxies of the present sample that have constant or slowly decaying SFR (half of the sample), the returned gas from the old stellar population is not a significant contribution and we can exclude that these galaxies were stripped of their gas at an old epoch.

As for the Local Group galaxies, the most striking aspect is the detection of an old population (> 10 Gyr) in almost all the galaxies of the sample. Only for FS76 the stellar population is consistent with a single burst at an intermediate age (6–7 Gyr). In some cases, the old population is not detected in the central extraction, but is seen in the $1 R_e$ extraction. This old population accounts for 15 to 80 per cent of the light and is the dominant fraction of the total mass of stars that has been formed: 70–90 per cent. The existence of populations contemporary of the old massive elliptical galaxies was already inferred from the detection of an old star cluster in a dE galaxy by Conselice (2006).

This implies that, though the environment is probably the key for quenching the star formation due to the stripping of the gas, its triggering is likely an internal process. But it also tells that most of the characteristics of the dEs were already set at an early epoch, certainly near or above $z \approx 1$. The diversity of observed SFH may be accounted for by different quenching times, and a residual star formation, fed by gas expelled by the evolved stars, may explain part of the SFR observed in the last few Gyr.

The lack of young galaxies, i. e. without old populations, is consistent with the non-detection of ‘dark’ galaxies by the blind HI survey ALFALFA (Kent et al. 2007). Apparently, all gas clouds that could make stars, did it in early epochs.

5.3 Central stellar populations

When seen at high spatial resolution (e. g. from HST/ACS data) most of the dEs display a nucleus, i. e. a light excess over a ‘reasonable’ extrapolation of the outer profile. This nucleus may either be redder or bluer than the surrounding population. The former case may be explained by a higher metallicity, while the latter could either be due to a younger age or to a lower metallicity (Lotz et al. 2004; Côté et al. 2006; Lisker et al. 2006). We will now discuss check if the presence of a nuclei is reflected in the stellar population and we will examine the two galaxies where a kinematically decoupled core is known, and we will review the central profiles of the populations in our sample.

5.3.1 Nucleated galaxies

Half of the galaxies of our sample are nucleated: FCC 46, 150, 207 245 and 266, FS 75 and 131 and NGC5898_DW2. These galaxies are evenly distributed along the sequence of

star formation timescale. No systematics stand out for the examination of the star formation history (Fig. 4) and of the gradients (Fig. 1 & 2). The four galaxies of the sample with the lowest central metallicity are nucleated (FCC 46, 207, 245 and NGC5898_DW2), and the correction of the line-of-sight contamination enhances slightly the effect (see Table 5). But two of the other nucleated galaxies have a rather high metallicity in their centres (about solar).

Beside the fact that half of the nuclei coincide with a low central metallicity, we cannot draw any conclusion concerning the nature of the nuclei, or the relation between the presence of a nucleus and the properties of the galaxy.

5.3.2 Galaxies with kinematically decoupled cores

FS076 and 373 host kinematically decoupled cores (KDCs) (De Rijcke et al. 2004) observed within $\lesssim 1 - 2$ arcsec. In FS373, the ellipticity profile of the isophotes suggests the presence of a small central stellar disc (De Rijcke et al. 2004). Within the central 3 arcsec the SSP-equivalent age raises regularly from 1.5 to 4.5 Gyr and the metallicity decreases from 0.1 to 0.35 dex. This behaviour is usual in our sample. The SFH reconstruction Table 6 and Fig. 4 reveals the presence of a young and high metallicity population contributing 25 per cent of the light in the central extraction, decreasing to 6 per cent in the $1 R_e$ aperture. Beside the KDC, FS76 exhibits other peculiarities. Its velocity dispersion, which initially rises with radius, starts to decline sharply outside one half-light radius. Moreover, its surface brightness profile is well described by a Sérsic law with index $n \approx 2$, making this galaxy more compact than most dEs of comparable luminosity ($M_B = -16.7$ mag). All this has been interpreted as evidence for a truncated dark halo and hence for the occurrence of tidal stripping (De Rijcke et al. 2001). As FS373, it has a regular metallicity profile decreasing from 0.2 to -0.2 dex within the central 3 arcsec and is consistent with a single burst about 6–7 Gyr ago in the both extractions.

The presence of a KDC does not appear to be reflected by any peculiarity of the stellar population. This indicates that the KDC is not linked with a recent event that would have been marked by star formation, and should instead be a long-lived feature. This supports the suggestion for a tidal origin discussed in De Rijcke et al. (2004).

5.3.3 Centrally depressed metallicity

We have shown above that the general trend is negative metallicity gradients at large scale. But in 5 cases we detect an opposite trend in the central region. Table 10 lists the galaxies with centrally depressed metallicity, with the magnitude of the effect and its radial extension. The central profiles of age does not display any systematics. As an illustration, Fig. 8 presents the profiles of FCC266.

Three of these objects are amongst those most dominated by an old population (short formation time-scale; FCC 266 245 and 136) outside of the depressed region their metallicity profile declines regularly, and they are round objects. The two others (FCC 288 and NGC5898_DW2) have flat metallicity profiles at large radii and contain an intermediate age or young populations; the last one has H_β emission, indicating residual ongoing star formation. They are flat objects.

Table 10. Centrally depressed metallicities. R_{max} is the radius, in arcsec and in pc (not deconvolved for seeing effect), where the metallicity reaches its maximum. $\Delta[\text{Fe}/\text{H}]$ is the amplitude of the metallicity depression between its maximum and the centre. For the last object of the table, FCC136, the detection is marginal.

Name	R_{max}		$\Delta([\text{Fe}/\text{H}])$ dex
	arcsec	pc	
FCC266	0.8	83	0.10
FCC245	2.0	208	0.50
NGC5898_DW2	1.0	160	0.40
FCC288	1.0	104	0.10
FCC136	0.7	73	0.10

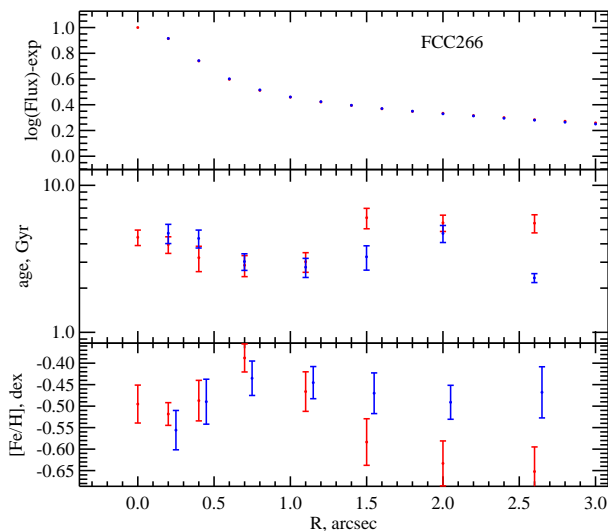


Figure 8. Central SSP-equivalent profiles of FCC266. The top panel is the excess over an exponential light profile fitted using the long-slit spectra in the region between 2 and 5 arcsec. The symbols are identical to Fig. 1. A finer radial binning than for Fig. 1 & 2 was achieved by targeting a lower S/N.

The metallicity depression can occur either in dE(di) objects or classical dEs. It seems somewhat independent of the large scale structure of the galaxy as well as the presence of a blue core (Lisker et al. 2006) or nucleus (Côté et al. 2006). Except for FCC245, whose peculiar profile is discussed in Appendix A, the depressed region is not clearly spatially resolved.

What interpretation to give to this phenomenon? As the seeing blurs the data in a 100 pc region, we cannot test if it is due to the characteristics of the nucleus or central cluster whose size is of 10 pc or less.

It is tempting to relate these depressions with the hypothesis that the dE nuclei are large globular clusters (Zinnecker et al. 1988) or mergers of clusters which decayed to the centre (Lotz et al. 2001).

Other explanations may be proposed. The mass of the nucleus is roughly proportional to the total mass of the galaxy and continue to low mass the relation between the masses of the super-massive black-hole and of its host (Wehner & Harris 2006; Ferrarese et al. 2006; Côté et al. 2006). The co-evolution that the similarity of the two kinds of central-mass concentration would imply, probably

imposes that the nuclei started to form early from low-metallicity gas and that its mean metallicity is at present comparable to the mean metallicity of the galaxy. Therefore, the nuclear metallicity of the nucleus is expected to be lower than that of the surrounding central region.

Another possibility is that the central star formation is partly sustained by pristine gas which lately cooled down. But the fact that depressions are observed in some objects where we do not detect any recent star formation seems to rule out this hypothesis.

5.4 Origin of the dwarf elliptical galaxies

Although high-speed gravitational interactions in a dense cluster environment can bring about the drastic morphological transformation from discy, gas-rich spirals or dIrrs to rounder, gas-poor dEs (Moore et al. 1998; Mastropietro et al. 2005), it remains to be seen whether the violent reshuffling of stellar orbits and induced star formation indeed lead to dEs presenting the characteristic metallicity gradients shown in this paper.

Another, more plausible, explanation is that dE galaxies are akin to dIrrs or BCDs but that the transformation is of a much more gentle nature than the “harassment” process. Other gas removing processes are “starvation” and “strangulation”, suggested by a.o. Larson et al. (1980); Tully & Trentham (2008); Kawata & Mulchaey (2008) and references therein. Once a gas-rich galaxy enters a cluster, the cluster potential imposes a Roche limit around this galaxy, making some of the hot gas unbound. This gas is no longer available for star formation. If the pressure of the intra-cluster medium (ICM) is strong enough, it may help to strip away this outer hot gas reservoir. Both processes are physically different but will most likely work in unison in any cluster/group environment. The outcome is in any case the same: the supply of gas cooling from the hot halo is cut off and the already accreted cold gas is transformed into stars until none is left. As a consequence, star formation peters out, leaving behind a gas-less dE with chemical and kinematical properties very similar to those of a dIrr.

Ram-pressure stripping (Gunn & Gott 1972; Roediger & Hensler 2005; Mayer et al. 2006) provides another means of removing gas from and consequently stopping star formation in gas-rich dwarf galaxies accreting onto a galaxy cluster or group. However, the efficiency of this mechanism, relative to starvation/strangulation, depends critically on the density of the intra-cluster or intra-group medium, a galaxy’s velocity relative to this medium, and the morphology of the infalling galaxy (round or discy). Based on a suite of simulations of spherically symmetric dwarf galaxies subjected to various ram-pressures, Mori & Burkert (2000) provide an expression for the critical dark-matter core mass above which, for a given ICM density and velocity, ram-pressure is not able to strip away the gas. Evaluating this critical mass for different clusters, it is clear that ram-pressure stripping of round dwarfs is a prominent process in Virgo and Coma-like environments but not in the Fornax cluster, the NGC5044 group or even less dense groups. Simulations using dwarf disc galaxies, on the other hand, show that even low-velocity, low-density ram-pressure is able to strip away the lion’s share of the gas in a time-scale of roughly 1 Gyr (Marcolini et al. 2003; Hester 2006). Boselli et al. (2008a,b)

show that the scaling relations of Virgo cluster dEs can be reproduced by ram-pressure stripping of low-luminosity spiral galaxies or BCDs. These authors could reject strangulation/starvation as the sole source of these relations. No conclusion could be reached regarding harassment because of the lack of enough N-body simulations of low-mass galaxies. The correlation between the age of the stellar population, estimated from absorption-line indices, and position within the Virgo cluster, suggests that the gas is being removed quickly from the infalling galaxies Michielsen et al. (2008).

It is clear that all these processes must act together in group/cluster environments. Which process is the dominant agent in removing gas from infalling dwarf galaxies depends on the characteristics of the cluster/group.

6 CONCLUSION

In this paper we bring observations of 16 dEs that can be confronted with the different scenario of formation and evolution of galaxies:

(i) The star formation in the present dEs started in the early Universe. The old population amounting for a dominant fraction of the mass is compatible with being co-eval of the oldest populations of massive elliptical galaxies, or bulges.

(ii) The star formation histories span a long time-scale. In general an intermediate age population (1-5 Gyr) is present, and often a tail of residual star formation extend to recent epochs. The more recent episodes of star formation are more concentrated than the old population.

(iii) The youngest sub-populations have higher metallicities, and in general the metallicity is decreasing from the centre outwards. The gradients are typically 0.5 dex/ R_e . This seems to be a common properties of dEs, shared by NGC205 (Koleva 2009). These gradients are seen in the old (10 Gyr) population. The steep metallicity gradients co-exist the age gradients (older outside) due to the effect of concentrating the star formation, resulting is shallower color gradients.

(iv) The flat and discy objects have almost constant metallicity. The absence of gradient may either be due of their particular geometry or may reflect a different origin like suggested by Lisker et al. (2006).

(v) We did not identify peculiarities in the stellar populations of the central region of the 2 galaxies with kinematically decoupled cores. But, in 5 galaxies we observe a depression of the metallicity in the core, that may be the signature of a blue core diluted by the seeing.

What can we conclude about the origin of dEs and the forces driving their evolution?

The prolonged star-formation history of dEs, compared with normal elliptical galaxies, is compatible with the idea of down-sizing (the shift of star formation to lower galaxy masses as cosmic time goes by). The old population of dEs, co-eval to that of more massive galaxies, may tell that the conditions to trigger the star formation in intrinsically small galaxies were satisfied independently of any strong environmental trigger. But alternatively, it may be compatible with the tidal harassment being the origin of the dEs, if this process can reproduce the other characteristics, and in particular the strong gradients.

The metallicity gradients in the old population indicates that it was not deeply mixed along its evolution. For instance, the flat metallicity profiles of massive elliptical galaxies is attributed to mergings: such an origin can certainly be excluded for the dEs, but also, tidal harassments must not erase the gradients if they are an important process to form dEs. The other environmental effects that can quench the star formation by removing the gas (ram-pressure stripping, starvation or strangulation Gunn & Gott 1972; Roediger & Hensler 2005; Mayer et al. 2006; Larson et al. 1980; Tully & Trentham 2008; Kawata & Mulchaey 2008) are more gentle and more likely to preserve the gradients.

These metallicity gradients are produced in simulations (Pelupessy et al. 2004; Stinson et al. 2007; Valcke et al. 2008) as a result of the self-regulation of the star formation by the stellar winds, but they generally settle on longer time scales and were not expected in the old population. At this point, more simulations would be required to try to reproduce these metallicity gradients.

The geometry of these galaxies is also certainly a key factor and is not well constrained by the present observations. A better understanding of the core region and of the disc galaxies requires to repeat stellar populations analyses using IFU spectroscopy (as was made for one galaxies by Chilingarian et al. 2007).

The co-existence of various classes of dEs (Lisker et al. 2006, 2007), the discy dEs having flat metallicity profiles, may result from the transformation, by the same environmental effects, a different progenitors, BCDs, dIrrs or small spiral galaxies.

From this present work and from other recent observation emerge a growingly consistent view of the formation of the diffuse dEs. The gas depleted dEs were once star forming and gas rich. The gas was exhausted by star formation, expelled by the winds and/or stripped by ram-pressure against the intra-cluster medium or by tidal interaction with other galaxies. During their 'active' live, the star formation was controlled by internal processes (feed-back) and by environmental effects which can trigger a burst thanks to the compression or finally finish it by cutting the gas supply.

ACKNOWLEDGMENTS

This paper is based on observations collected at the European Southern Observatory, Paranal, Chile (programs 165.N-0115, 075.B-0179, and 076.B- 0196). MK acknowledges a PhD grant from the French Embassy in Sofia. SDR is a postdoctoral fellow with the National Science Fund – Flanders (FWO). This project was supported by a Tournesol Scientific Exchange Programme between the Flemish Community and France.

We are deeply indebted to Anna Pasquali, Victor P. Debattista and Ignacio Ferreras who initiated this observational program. We thank Pierre Ocvirk for providing publicly the STECKMAP package, and Eric Emsellem for fruitful discussions. We also thank the anonymous referee for his/her suggestions and comments.

REFERENCES

- Alard C., 2001, *A&A*, 377, 389
- Barazza F. D., Binggeli B., Jerjen H., 2002, *A&A*, 391, 823
- Battaglia G., Tolstoy E., Helmi A., Irwin M. J., Letarte B., Jablonka P., Hill V., Venn K. A., Shetrone M. D., Arimoto N., Primas F., Kaufer A., Francois P., Szeifert T., Abel T., Sadakane K., 2006, *A&A*, 459, 423
- Boselli A., Boissier S., Cortese L., Gavazzi G., 2008a, *ApJ*, 674, 742
- , 2008b, *A&A*, 489, 1015
- Bouchard A., Jerjen H., Da Costa G. S., Ott J., 2007, *AJ*, 133, 261
- Buyle P., De Rijcke S., Michielsen D., Baes M., Dejonghe H., 2005, *MNRAS*, 360, 853
- Chilingarian I. V., Prugniel P., Sil'chenko O. K., Afanasiev V. L., 2007, *MNRAS*, 376, 1033
- Cid Fernandes R., Mateus A., Sodré L., Stasińska G., Gomes J. M., 2005, *MNRAS*, 358, 363
- Coelho P., Barbuy B., Meléndez J., Schiavon R. P., Castilho B. V., 2005, *A&A*, 443, 735
- Cole A. A., Skillman E. D., Tolstoy E., Gallagher III J. S., Aparicio A., Dolphin A. E., Gallart C., Hidalgo S. L., Saha A., Stetson P. B., Weisz D. R., 2007, *ApJ*, 659, L17
- Conselice C. J., 2006, *ApJ*, 639, 120
- Côté P., Piatek S., Ferrarese L., Jordán A., Merritt D., Peng E. W., Hasegan M., Blakeslee J. P., Mei S., West M. J., Milosavljević M., Tonry J. L., 2006, *ApJS*, 165, 57
- Davidge T. J., 2005, *AJ*, 130, 2087
- De Rijcke S., Dejonghe H., Zeilinger W. W., Hau G. K. T., 2001, *ApJ*, 559, L21
- , 2003a, *A&A*, 400, 119
- , 2004, *A&A*, 426, 53
- De Rijcke S., Michielsen D., Dejonghe H., Zeilinger W. W., Hau G. K. T., 2005, *A&A*, 438, 491
- De Rijcke S., Zeilinger W. W., Dejonghe H., Hau G. K. T., 2003b, *MNRAS*, 339, 225
- Dolphin A. E., 2002, *MNRAS*, 332, 91
- Dolphin A. E., Saha A., Skillman E. D., Dohm-Palmer R. C., Tolstoy E., Cole A. A., Gallagher J. S., Hoessel J. G., Mateo M., 2003, *AJ*, 126, 187
- Ferguson H. C., Binggeli B., 1994, *A&A Rev.*, 6, 67
- Ferrarese L., Côté P., Dalla Bontà E., Peng E. W., Merritt D., Jordán A., Blakeslee J. P., Hasegan M., Mei S., Piatek S., Tonry J. L., West M. J., 2006, *ApJ*, 644, L21
- Geha M., Guhathakurta P., van der Marel R. P., 2003, *AJ*, 126, 1794
- Goto T., Yamauchi C., Fujita Y., Okamura S., Sekiguchi M., Smail I., Bernardi M., Gomez P. L., 2003, *MNRAS*, 346, 601
- Gourgoulhon E., Chamaroux P., Fouque P., 1992, *A&A*, 255, 69
- Graham A. W., Guzmán R., 2003, *AJ*, 125, 2936
- Graham A. W., Jerjen H., Guzmán R., 2003, *AJ*, 126, 1787
- Grebel E. K., 2000, in *Bulletin of the American Astronomical Society*, Vol. 32, pp. 698–
- Gunn J. E., Gott J. R. I., 1972, *ApJ*, 176, 1
- Haines C. P., Gargiulo A., La Barbera F., Mercurio A., Merluzzi P., Busarello G., 2007, *MNRAS*, 381, 7
- Heavens A. F., Jimenez R., Lahav O., 2000, *MNRAS*, 317, 965
- Hester J. A., 2006, *ApJ*, 647, 910
- Jerjen H., Kalnajs A., Binggeli B., 2000, *A&A*, 358, 845
- Kawata D., Mulchaey J. S., 2008, *ApJ*, 672, L103
- Kent B. R., Giovanelli R., Haynes M. P., Saintonge A., Stierwalt S., Balonek T., Brosch N., Catinella B., Koopmann R. A., Momjian E., Spekkens K., 2007, *ApJ*, 665, L15
- Koleva M., 2009, PhD thesis, University of Lyon
- Koleva M., Gupta R., Prugniel P., Singh H., 2008a, in *Astronomical Society of the Pacific Conference Series*, Vol. 390, *Pathways Through an Eclectic Universe*, Knapen J. H., Mahoney T. J., Vazdekis A., eds., pp. 302–
- Koleva M., Prugniel P., De Rijcke S., 2008b, *Astronomische Nachrichten*, 329, 968
- Koleva M., Prugniel P., Ocvirk P., Le Borgne D., Soubiran C., 2008c, *MNRAS*, 385, 1998
- Kormendy J., 1985, *ApJ*, 295, 73
- Kormendy J., Fisher D. B., Cornell M. E., Bender R., 2008, arXiv:0810.1681
- Kroupa P., Tout C. A., Gilmore G., 1993, *MNRAS*, 262, 545
- Larson R. B., Tinsley B. M., Caldwell C. N., 1980, *ApJ*, 237, 692
- Le Borgne D., Rocca-Volmerange B., Prugniel P., Lançon A., Fioc M., Soubiran C., 2004, *A&A*, 425, 881
- Lee H., Skillman E. D., Venn K. A., 2006, *ApJ*, 642, 813
- Li Z., Han Z., 2008, *ApJ*, 685, 225
- Lisker T., Glatt K., Westera P., Grebel E. K., 2006, *AJ*, 132, 2432
- Lisker T., Grebel E. K., Binggeli B., Glatt K., 2007, *ApJ*, 660, 1186
- Lotz J. M., Miller B. W., Ferguson H. C., 2004, *ApJ*, 613, 262
- Lotz J. M., Telford R., Ferguson H. C., Miller B. W., Stivavelli M., Mack J., 2001, *ApJ*, 552, 572
- Mac Low M.-M., Ferrara A., 1999, *ApJ*, 513, 142
- Mapelli M., Ripamonti E., Tolstoy E., Sigurdsson S., Irwin M. J., Battaglia G., 2007, *MNRAS*, 380, 1127
- Marcolini A., Brighenti F., D'Ercole A., 2003, *MNRAS*, 345, 1329
- Marcolini A., D'Ercole A., Battaglia G., Gibson B. K., 2008, *MNRAS*, 386, 2173
- Martínez-Delgado D., Aparicio A., Gallart C., 1999, *AJ*, 118, 2229
- Mastropietro C., Moore B., Mayer L., Debattista V. P., Piffaretti R., Stadel J., 2005, *MNRAS*, 364, 607
- Mayer L., Governato F., Colpi M., Moore B., Quinn T., Wadsley J., Stadel J., Lake G., 2001, *ApJ*, 547, L123
- Mayer L., Mastropietro C., Wadsley J., Stadel J., Moore B., 2006, *MNRAS*, 369, 1021
- Michielsen D., Boselli A., Conselice C. J., Toloba E., Whiley I. M., Aragón-Salamanca A., Balcells M., Cardiel N., Cenarro A. J., Gorgas J., Peletier R. F., Vazdekis A., 2008, *MNRAS*, 385, 1374
- Michielsen D., De Rijcke S., Zeilinger W. W., Prugniel P., Dejonghe H., Roberts S., 2004, *MNRAS*, 353, 1293
- Michielsen D., Koleva M., Prugniel P., Zeilinger W. W., De Rijcke S., Dejonghe H., Pasquali A., Ferreras I., Debattista V. P., 2007, *ApJ*, 670, L101
- Moore B., Lake G., Katz N., 1998, *ApJ*, 495, 139
- Mori M., Burkert A., 2000, *ApJ*, 538, 559
- Moultaka J., 2005, *A&A*, 430, 95
- Nieto J.-L., Prugniel P., 1987, *A&A*, 186, 30

- Ocvirk P., Pichon C., Lançon A., Thiébaud E., 2006, MNRAS, 365, 74
- Pasquali A., Larsen S., Ferreras I., Gnedin O. Y., Malhotra S., Rhoads J. E., Pirzkal N., Walsh J. R., 2005, AJ, 129, 148
- Paturel G., Petit C., Prugniel P., Theureau G., Rousseau J., Brouty M., Dubois P., Cambrézy L., 2003, A&A, 412, 45
- Pelupessy F. I., van der Werf P. P., Icke V., 2004, A&A, 422, 55
- Prugniel P., Golev V., Maubon G., 1999, A&A, 346, L25
- Prugniel P., Koleva M., Ocvirk P., Le Borgne D., Soubiran C., 2007a, in IAU Symposium, Vol. 241, IAU Symposium, Vazdekis A., Peletier R. F., eds., pp. 68–72
- Prugniel P., Simien F., 2003, Ap&SS, 284, 603
- Prugniel P., Soubiran C., 2001, A&A, 369, 1048
- Prugniel P., Soubiran C., Koleva M., Le Borgne D., 2007b, arXiv:astro-ph/0703658
- Rieschick A., Hensler G., 2003, Ap&SS, 284, 861
- Roediger E., Hensler G., 2005, A&A, 433, 875
- Sánchez-Blázquez P., Peletier R. F., Jiménez-Vicente J., Cardiel N., Cenarro A. J., Falcón-Barroso J., Gorgas J., Selam S., Vazdekis A., 2006, MNRAS, 371, 703
- Stinson G. S., Dalcanton J. J., Quinn T., Kaufmann T., Wadsley J., 2007, ApJ, 667, 170
- Thomas D., Bender R., Hopp U., Maraston C., Greggio L., 2003a, Ap&SS, 284, 599
- Thomas D., Maraston C., Bender R., 2003b, MNRAS, 339, 897
- Tojeiro R., Heavens A. F., Jimenez R., Panter B., 2007, MNRAS, 381, 1252
- Tully R. B., Trentham N., 2008, AJ, 135, 1488
- Valcke S., de Rijcke S., Dejonghe H., 2008, MNRAS, 389, 1111
- van den Bosch F. C., Aquino D., Yang X., Mo H. J., Pasquali A., McIntosh D. H., Weinmann S. M., Kang X., 2008, MNRAS, 387, 79
- van Zee L., Skillman E. D., Haynes M. P., 2004, AJ, 128, 121
- Wehner E. H., Harris W. E., 2006, ApJ, 644, L17
- Wheeler J. C., Sneden C., Truran Jr. J. W., 1989, ARA&A, 27, 279
- Young L. M., Lo K. Y., 1997, ApJ, 476, 127
- Zinnecker H., Keable C. J., Dunlop J. S., Cannon R. D., Griffiths W. K., 1988, in IAU Symposium, Vol. 126, The Harlow-Shapley Symposium on Globular Cluster Systems in Galaxies, Grindlay J. E., Philip A. G. D., eds., pp. 603–+

APPENDIX A: GALAXY BY GALAXY DESCRIPTION

This Appendix gathers comments on individual objects written down during the spectroscopic analysis. We briefly discuss the of the SFH in 1 arcsec and $1R_e$, and the SSP-equivalent parameters of the 'corrected' from the light on the line-of-sight inner regions in each object. Except when explicitly noted, we chose the SFH on the basis of the goodness and stability of the fit. Usually there was no particular spectral features which drove our choice of the SFH. It was more matter of general smaller residuals (i. e. smaller χ^2).

FCC043. The inner 1 arcsec of FCC043 is well described with one coeval population at intermediate age and metallicity. In the outer part ($1R_e$ extraction) we find a metal poor old component (30per cent in light). We were unable to subtract the contamination of the light on the line-of-sight from the 1 arcsec extraction.

The spectrum is contaminated by a background object about 20 arcsec East of the centre: The emission line at 4488 Å (in the galaxy rest-frame) seen between 17 and 24 arcsec is probably [OIII] $\lambda 3727\text{Å}$ redshifted at $z=0.21$. The residuals show H_δ in absorption and H_γ in absorption plus emission. We excluded the contaminated spectra from the analysis.

FCC046 This galaxy has emission in H_β and [OIII]. It is nucleated and is detected in HI. We could distinguish 4 populations in both the 1 arcsec and $1R_e$ extractions. The light fraction of the oldest population is 20-22per cent (for the 1 arcsec and $1R_e$ extractions respectively). Its star formation history reveals a strong bursts at 12 Gyr (much metal poor), small residual star-formation during the middle ages and a new present strong star formation with solar metallicity, more prominent in the centre. Another indication of the mix of young and old population is the HeI 4388Å line, due to hot stars, which is better fitted in the case of multiple SSPs. The correction from the light on the line-of-sight reveals more metal-poor population.

FCC136 This flat, S0 galaxy has a small amount of intermediate stars in the centre. The SSP-equivalent ages and metallicities of the corrected spectrum are smaller than in the 1 arcsec extraction. In the outer part we could not detect anything but old population.

FCC150 The inner 1 arcsec of this galaxy displays old and intermediate component. The corrected inner part is slightly more metal-poor and younger than the uncorrected 1 arcsec parameters. Curiously we were able to detect young component in the outer region, but not in the inner.

FCC204 This is a galaxy with a spiral structure. The SFH in the both $1R_e$ and 1 arcsec extractions are consistent with two subpopulations of old and intermediate ages.

FCC207 The inner part of this galaxy displays constant SFH till recent epochs. The presence of a young population is marked by Balmer and [OIII] emissions. In the $1R_e$ region we failed to find a young component.

FCC245 This galaxy is best fitted with a two-population (intermediate and old) scenario. Its corrected core shows a decline in the SSP-equivalent metallicity and age. The SSP profiles of FCC245 are peculiar. It is the galaxy with the best evidence for a central metallicity depression. The metallicity in the centre is about -0.8 dex, it is peaking at -0.5 dex between $r = 1.4$ and 4 arcsec, and decreases after to -0.8 again (Fig. A1). The SFH indicates the presence of an old population of metallicity -1 dex with an intermediate one overimposed.

We extracted the spectra in $r = 1.3$ to 4 arcsec and studied the SFH. In order to ease the comparison with the other extractions we fixed the old population to 12 Gyr, $[\text{Fe}/\text{H}]=-1$ dex. We find almost the same population mix in the central and $1R_e$ extractions, with an intermediate age population aged about 1.5 Gyr and a super-solar metallicity

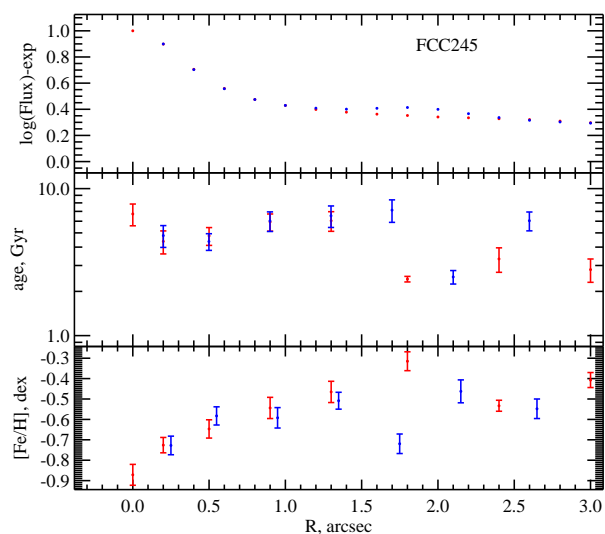


Figure A1. Central SSP-equivalent profiles of FCC245. The top panel is the excess over an exponential light profile fitted using the long-slit spectra in the region between 2 and 5 arcsec. The symbols and binning are identical to Fig. 8.

$[\text{Fe}/\text{H}] = +0.4$ dex amounting 25 per cent of the light. In the middle extraction the intermediate population is also the same, but has a fraction of 35 per cent of the light. This SFH accounts reasonably for the observed SSP profiles.

It looks like if this dE0 has a ring with an enhanced intermediate population. But the photometry does not provide any hint for such a feature.

FCC266 This is a nucleated dE. We detect a small fraction of young population in 1 arcsec and $1R_e$, but it is going to the age low limit. We adopted a 2-bursts fit. When subtracting the line-of-sight contamination of the light we was left with only noise and we could not fit any SSP to it.

The North side of the galaxy spectrum is contaminated by a background barred spiral galaxy located at red-shift 0.23, having an SSP-equivalent age of 2.5 Gyr and solar metallicity. We did not attempt to decontaminate the spectra and simply excluded the region beyond 5 arcsec on that side.

FCC288 A spiral structure is found in FCC288. In the outer part we detect a young population which is not seen in the inner 1 arcsec (like in the case of FCC150). In the both extractions the Mg_b is over-fitted, which suggests slight α -under-abundance in comparing to our models (with solar neighborhood abundance, Wheeler et al. 1989).

DW1 In the inner arcsecond the two-components population (old plus intermediate age) give the best and more stable fit (in χ^2 sense). For the $1R_e$ the situation is more complex since if we adopt the three population fit the young component goes to the high metallicity limit. On the other side, the fit is worse when only two populations are considered. So, even if with an uncomfortably high metallicity we keep the three bursts model. The corrected inner part have lower SSP-equivalent metallicity and age in comparison with the non-corrected one burst fit to 1 arcsec.

DW2 This galaxy has a similar SFH as FCC046. Actively star forming at old ages and at present and more quiet at

intermediate ages. The SSP-equivalent fit is considerably worse with strong residuals at G4300, Fe and Mg lines. A SSP obviously does not match the observation. In the corrected 1 arcsec we find an young population with low metallicity.

FS29 The best SFH for this galaxy seems to be represented by an intermediate and old burst. In central 1 arcsec the star formation seems to be more constant, while in the outer part it is rapidly diminishing.

FS75 The outer $1R_e$ shows a small component but the metallicity is not constrained (too big error bars) and we adopted the two bursts fit. Indeed it also has strong Balmer and oxygen emission lines. It is one of the rare cases, where the corrected 1 arcsec is more metal-rich than the uncorrected.

FS131 This is a peanut shaped galaxy which is also marked as nucleated. We could not resolve more than one population in the central 1 arcsec, even when we tried to correct for the outside light contamination. In the outer regions however we see some fast decreasing SFH, composed from an old and intermediate population.

FS373 This galaxy was resolved in 3 populations. While in the centre the intermediate age burst is dominating the mass, it has the smallest contribution in the outskirts. Both extractions show emission in $[\text{OII}]$. The S/N was not sufficient to obtain SSP parameters for the corrected 1 arcsec.